

A suite of benchmark and challenge problems for enhanced geothermal systems

Mark White  · Pengcheng Fu · Mark McClure · George Danko · Derek Elsworth · Eric Sonnenthal · Sharad Kelkar · Robert Podgorney

Received: 20 June 2017 / Accepted: 23 October 2017

© Springer International Publishing AG, part of Springer Nature (outside the USA) 2017

Abstract A diverse suite of numerical simulators is currently being applied to predict or understand the performance of enhanced geothermal systems (EGS). To build confidence and identify critical development needs for these analytical tools, the United States Department of Energy, Geothermal Technologies Office sponsored a Code Comparison Study (GTO-CCS), with participants from universities, industry, and national laboratories. A principal objective for the study was to create a community forum for improvement and verification of numerical simulators for EGS modeling. Teams participating in the study were those representing U.S. national laboratories, universities, and industries, and each team brought unique numerical simulation capabilities to bear on the problems.

Two classes of problems were developed during the study, benchmark problems and challenge problems. The benchmark problems were structured to test the ability of the collection of numerical simulators to solve various combinations of coupled thermal, hydrologic, geomechanical, and geochemical processes. This class of problems was strictly defined in terms of properties, driving forces, initial conditions, and boundary conditions. The challenge problems were based on the enhanced geothermal systems research conducted at Fenton Hill, near Los Alamos, New Mexico, between 1974 and 1995. The problems involved two phases of research, stimulation, development, and circulation in two separate reservoirs. The challenge problems had specific questions to be

M. White (✉)

Geosciences Group, Pacific Northwest National Laboratory, Richland, WA, USA
e-mail: mark.white@pnl.gov

P. Fu

Computational Geosciences, Lawrence Livermore National Laboratory, Livermore, CA, USA
e-mail: fu4@llnl.gov

M. McClure

McClure Geomechanics, Palo Alto, CA, USA
e-mail: mark@mccluregeomechanics.com

G. Danko

Mining and Metallurgical Engineering, University of Nevada, Reno, Reno, NV, USA
e-mail: danko@unr.edu

D. Elsworth

Energy and Mineral Engineering, Pennsylvania State University, State College, PA, USA
e-mail: elsworth@psu.edu

E. Sonnenthal

Earth and Environmental Sciences, Lawrence Berkeley National Laboratory, Berkeley, CA, USA
e-mail: elsonnenthal@lbl.gov

S. Kelkar

HydroGeoLogic Inc., Las Vegas, NV, USA
e-mail: sharadmkelkar@gmail.com

R. Podgorney

Energy Systems and Technologies Division, Idaho National Laboratory, Idaho Falls, ID, USA
e-mail: robert.podgorney@inl.gov

answered via numerical simulation in three topical areas: (1) reservoir creation/stimulation, (2) reactive and passive transport, and (3) thermal recovery. Whereas the benchmark class of problems were designed to test capabilities for modeling coupled processes under strictly specified conditions, the stated objective for the challenge class of problems was to demonstrate what new understanding of the Fenton Hill experiments could be realized via the application of modern numerical simulation tools by recognized expert practitioners. We present the suite of benchmark and challenge problems developed for the GTO-CCS, providing problem descriptions and sample solutions.

Keywords Enhanced geothermal systems · Numerical simulation · Code comparison · Coupled process modeling

1 Introduction

Enhanced geothermal systems (EGS) are a promising yet currently under-tapped energy resource (Wood 2009). Extracting thermal energy from the deep subsurface can be accomplished in a seemingly straightforward fashion (i.e., drilling a pair of wells to depths where rock temperatures approach 300 °C, fracturing and hydraulically connecting the rock between the wells, and circulating a fluid from one well to the other in a closed system through the hydraulic connection). Potential fluids are natural brines, compressed CO₂, or exotic liquid mixtures, including those with nanoparticles. The heated fluid flashes to steam at ambient surface pressures or exchanges heat with a working fluid, which vaporizes during the heat exchange process and subsequently drives an electricity-producing turbine. The cooled fluid is re-injected into the thermal reservoir directly, or further cooled via secondary heat recovery systems (e.g., building heating). Although conceptually straightforward, like geologic sequestration of greenhouse gases, EGS presents challenges, including understanding the fracture-dominated flow network, delaying thermal drawdown through tailored production scheduling, studying the feasibility of alternative working fluid, managing induced seismicity, etc. (Jeanloz and Stone 2013), to fully realize this

energy resource. Mathematical models and numerical simulation are the analytical tools that will be used to help meet these challenges, evaluate the feasibility of EGS at various geothermal sites, and will be essential in designing and evaluating operations of geothermal systems. To establish the credibility of numerical simulators as practical analytical tools, it is essential to demonstrate their capabilities for accurately and reliably modeling EGS processes both individually and coupled. A common approach to evaluating numerical simulators, which contributes to their acceptance as practical analytical tools, is to exercise a suite of numerical simulators on problems that consider key processes of interest—to conduct a code comparison study.

The United States Department of Energy (DOE), Geothermal Technologies Office (GTO) recently sponsored a code comparison study (GTO-CCS) to create a community forum for EGS reservoir modeling code improvement and verification, building confidence in the suite of available numerical tools, and ultimately identifying critical future development needs for the geothermal modeling community. Numerical simulation is a key method for understanding the creation and evolution of EGS. The development of predictive numerical tools has paralleled roughly four decades of growth of EGS concepts and technology, as well as studies of other unconventional subsurface energy and geologic carbon sequestration settings. These are complex geologic environments where thermodynamics, hydrodynamics, rock mechanics, and geochemistry all contribute critically to system behavior across disparate lengths and time scales. The usefulness of numerical tools in these settings is moderated by confidence in the quality of the results they produce. Validation with analytical solutions, laboratory and field data, and inter-comparisons with other codes is therefore crucial to ensure that simulation can contribute robustly to EGS development. The principal issues of concern for this study were to determine (1) whether valid mathematical models for the fundamental processes associated with geothermal technologies exist, and (2) whether available numerical simulators assimilate these models to yield reliable and accurate numerical solutions to problems involving conditions of practical interest.

The GTO-CCS comprised two stages; the first (GTO-CCS Problems) (White et al. 2016b) where participants developed and addressed a series of

benchmark problems, and the second (GTO-CCS Challenge Problems) (White et al. 2017) where more challenging problems, extracted from real EGS field studies, were developed and considered. During the first stage of the study seven benchmark problems were chosen by the participants, with each problem having a champion. Benchmark problems were designed to investigate specific coupled processes relevant to enhanced geothermal systems. This stage of the study was completed during the first year, and documented in four papers at the Fortieth Workshop on Geothermal Reservoir Engineering, held at Stanford University, Stanford, California, January 26–28, 2015 (Bahrami et al. 2015; Ghassemi et al. 2015; White and Phillips 2015; White et al. 2015). The principal conclusions from this work were that while the U.S. EGS simulation community has a diverse set of computational tools with respect to conceptual approaches and numerical implementations, they are able to simulate coupled subsurface processes with comparable results. The evolution of numerical simulators over the last 35 years, since the 1980 geothermal code comparison study (Molloy et al. 1980) has been impressive, but work remains to be done. Uncertainties in simulation results as measured by the ISO-13528 standard tend to increase with the number of coupled processes in the problem and the modeling of strongly coupled THMC processes remains challenging. The collaborative nature of this study has formed the foundation for the EGS simulation community to collectively address field-scale systems, where coupled process modeling will be essential for understanding the system and experimental observations. Confidence in numerical simulation grows from agreement among field experts, especially when diverse perspectives are represented. This study yielded convergence in understanding over the course of each problem via open dialogue and discussions among the participants.

During the Challenge Problems stage of the GTO-CCS, challenge problems were developed based on the research activities conducted at the Fenton Hill Hot Dry Rock (HDR) Test Site, referred to by the Los Alamos Scientific Laboratory (LASL) [now the Los Alamos National Laboratory (LANL)] as Technical Area 57 (TA-57), or more simply as Fenton Hill (Brown et al. 2012). Fenton Hill is located about 1.9 miles west of the main ring-fracture of the Valles Caldera in the Jemez Mountains of north-central New

Mexico, USA. Principal research activities at Fenton Hill took place in two HDR reservoirs. Development and testing in the Phase I Reservoir occurred between 1973 and 1980, over the approximate depth interval from 3000 to 10,000 ft (871–3064 m) at temperatures between 105 and 205 °C. In contrast, the Phase II Reservoir activities spanned from 1979 through 1995 at greater depths and higher temperatures, over the approximate depth interval from 12,000 to 14,000 ft (3600–4200 m) at temperatures between 260 and 317 °C. In terms of Holling's classification (Holling 1978) of modeling problems the GTO-CCS Challenge Problems are data rich with respect to the details about the experiments conducted at the Fenton Hill Test Site thanks to the recent publication by Brown et al. (2012), but at the same time data limited with respect the rock mass. Even critical information about the stress state in both reservoirs remain uncertain, which puts the GTO-Challenge Problems in the realm of data-limited modeling problems. Starfield and Cundall (1988) state that “the purpose of modeling data-limited problems is to gain understanding and explore potential trade-offs and alternatives, rather than to make absolute predictions.” The desired outcome for the GTO-CCS Challenge Problems is that the modeling efforts yield new understanding or interpretations of the complex coupled processes that occurred during the Fenton Hill experiments, and hopefully that a collective agreement is found among the field experts often with diverse modeling approaches and capabilities. Available data sets for these problems are described in detail in White et al. (2015).

The problem sets in both phases are aimed to address a key difference between EGS and conventional hydrothermal resources. Fluid flow in the former is dominated by fracture networks whereas heat transport is primarily through conduction from the largely impermeable rock to the working fluid. In hydrothermal systems, however, convective heat transport dominates as fluid flows through the porous, hot, rock medium. Another critical aspect of EGS development is induced seismicity. Imaging seismic events induced by fluid injection has been a crucial technique for characterizing the stimulated fracture network since the Fenton Hill experiment (Brown et al. 2012; Majer et al. 2007). On the other hand, earthquakes of magnitudes large enough to cause public concerns to have also been linked to EGS development (Deichmann and Giardini 2009) and

other forms of fluid injection. Although the problems sets do not directly address the problem of induced seismicity, the physical mechanism, namely fracture/fault slipping caused by stress/pressure alteration (McClure and Horne 2011), is a key theme of many problems.

Numerical modeling approaches for EGS applied during the GTO-CCS can be divided into three broad categories: (1) discrete fracture, (2) effective continuum, and (3) reduced order. The discrete fracture approach considers fluid flow within individual fractures (McClure and Horne 2013); whereas, the effective continuum approach converts contributions of individual fractures into effective properties applied over volumetric grid cells (Kazemi et al. 1976; Lemonnier and Bourbiaux 2010; Warren and Root 1963). The reduced order approach involves the development of response functions from the execution of either discrete fracture or effective continuum based approaches. General modeling approaches will be described for each of the three broad categories, including governing and constitutive equations, numerical solution schemes, and coupling schemes for the four major EGS processes: (1) thermal, (2) hydrologic, (3) geomechanical, and (4) geochemical. Presentation of the general modeling approaches provides readers with clearer understanding of the core concepts and foundational scales for modeling. This review of general approaches is followed with brief descriptions of the individual computer codes used in the GTO-CCS. These descriptions of individual codes are not exhaustive, but references to other publications or user's manuals are cited for the interested reader. Detailed descriptions of process models and numerical approaches are beyond the scope of this manuscript, but can be found in the companion technical documents for the study (White et al. 2016b, 2017).

2 Participants and codes

Participation in the code comparison study was solicited by email and announcements at two consecutive Stanford Geothermal Workshops. As discussed above, one-day workshop was held at Stanford University, following the 2013 Stanford Geothermal Workshop, at which the structure of the study was discussed and problems were proposed in two

categories: benchmark and challenge (Scheibe et al. 2013). A study kickoff meeting was held during the 2014 Stanford Geothermal Workshop to announce the schedule for the study and introduce participants. Problem champions were assigned to each of the proposed benchmark problems. Problem champions were responsible for developing problem descriptions, submitting initial results, and leading results discussions. Results for the benchmark problems were submitted by 11 teams. Although the study was open to international teams, all participating teams had U.S. affiliations and were from universities, national laboratories, and industry. Team affiliations, members and computer codes are shown in Table 1. The first requirement for all participating teams was to document the codes being applied to the benchmark problems on the GTO-Velo code catalog. A synopsis of the code catalog is shown in Table 2, which lists the code name, code developer(s), modeled process classes, key capabilities, spatial and temporal discretization methods or numerical solution approaches, and primary applications. It should be noted that many codes that participating this study are large-scale research codes that have relatively large teams of developers and solve problems not limited to EGS. Table 2 only lists the key authors and code features directly relevant to this study.

The study schedule was organized around weekly teleconferences/web-conferences. A minimum of three teleconferences/web-conferences were dedicated to each of the benchmark problems: (1) problem description by the problem champion, (2) preliminary result submission and discussions, and (3) final result submission and discussions. Each participating team had the opportunity to present an overview of the computer code(s) they would be applying during the study. A number of the benchmark problems required alterations from their original forms to make them either more specific, to include additional parameters, or to be more approachable across the suite of computer codes. Three of the weekly teleconferences/web-conferences were used to define challenge problems that would be proposed for a sequential study. Participating teams were given the freedom to submit or not submit solutions to the problems, but a diverse suite of solution approaches was sought and encouraged for each problem.

Table 1 GTO-CCS teams and computer codes

Team affiliation	Team members	Code(s)
Idaho National Laboratory (INL)	Robert Podgorney, Hai Huang, Mitch Plummer, Yidong Xia	FALCON
Itasca Consulting Group (Itasca)	Jason Furtney, Christine Detournay, Azadeh Riahi, Branko Damjanac	FLAC3D
Lawrence Berkeley National Laboratory (LBNL)	Jonny Rutqvist, Eric Sonnenth, Jens Birkholzer	TOUGH, FLAC3D
Lawrence Livermore National Laboratory (LLNL)	Charles Carrigan, Pengcheng Fu, Bin Guo, Yue Hao	NUFT, GEOS
Los Alamos National Laboratory (LANL)	Sharad Kelkar	FEHM
McClure Geomechanics, LLC (McCG)	Mark McClure	CFRAC
Oak Ridge National Laboratory (ORNL)	Charlotte Barbier, Yarom Polsky	PFLOTRAN
The University of Oklahoma (OU)	Ahmad Ghassemi, Qinglu Cheng, Kai Huang, M.R. Safari, Varahanaresh Sesetty, Qingfeng Tao	GeoFrac-Mech, GeoFrac-Stim
Pacific Northwest National Laboratory (PNNL)	Mark White, Signe White, Diana Bacon, Tim Scheibe	STOMP
Pennsylvania State University (PSU)	Derek Elsworth, Yi Fang, Quan Gan, Hiroyuki Honda Kyungjae Im, Baisheng Zheng,	TOUGHREACT, FLAC3D
Stanford University (Stanford)	Roland Horne, Jack Norbeck, Yang Wong	CFRAC-Stanford, GPRS
The University of Texas at Austin (UTA)	Mark McClure, Kit-Kwan Chiu	CFRAC-UT
University of Nevada, Reno (UNR)	George Danko, Davood Bahrami	MULTIFLUX, TOUGH2, NUFT, 3DEC

3 Benchmark problems

In 1980 the geothermal community dedicated the annual Geothermal Reservoir Engineering workshop (Molloy et al. 1980) to defining an appropriate role for numerical simulation in terms of investment decisions related to geothermal performance predictions and to assessing the state of development of geothermal reservoir numerical simulators. The technical foundation for achieving the workshop objectives was a code comparison study, which involved six geothermal problems. Whereas the suite of problems considered a variety of geometric configurations and petrophysical property distributions, the principal processes of concern were single-phase flow, two-phase flow, single-phase to two-phase flash, and heat transfer (i.e., TH processes). The current study (GTO-CCS) is similar to the 1980 code comparison study in that the objectives are nearly unchanged: an assessment of computer codes for predicting the power production

potential and longevity of geothermal reservoirs. Today's numerical simulators for EGS, however, have evolved from those of the 1980 s, particularly with respect to modeling coupled processes. In alignment with this transition in simulation capabilities, all of the benchmark problems in this study included coupled process elements of either HM, THM, or THC, as summarized in Table 3. Problem descriptions provided in this manuscript are limited, but more complete descriptions are provided in the companion technical document (White et al. 2016b).

3.1 Benchmark problem 1: poroelastic/thermal transport in a single fracture

3.1.1 Problem champion: Robert Podgorney, Idaho National Laboratory

Benchmark Problem 1 was loosely based on recent observations at a test well from the Raft River EGS

Table 2 Code characteristics

Code + developer(s)	Class type	Key capabilities	Spatial and temporal discretization	Primary application
3DEC (Distinct-Element Modeling of Jointed and Blocky Material in 3D) + Peter Cundall	M	Discontinuous Medium Modeled as an Assemblage of Convex Polyhedra or Concave Polyhedra + Rigid or Deformable Blocks + Linear and Nonlinear Force Displacement Relations for Normal and Shear Direction + Elastic, Anisotropic + Mohr–Coulomb, Drucker Prager, Bilinear Plasticity, and Strain-Softening Material Models	3D + Explicit Time Marching Solution + Automatic Mesh Generation in Fully Deformable Blocks + Automatic Time Step Calculator	Advanced geotechnical analysis of soil, rock, and structural support in three dimensions and the response of discontinuous media subject to static or dynamic loading
CFRAC_Stanford (Complex Fracturing ReseArch Code) + Roland Horne and Jack Norbeck	THM	Continuum-Elastic + Discrete Fractures + Fracture Propagation + Displacement-Based Governing Equations + Stress-Dependent Permeability	2D Structured + Finite Difference + Implicit Temporal	Modeling evolution of geomechanics-driven permeability evolution
CFRAC_UT (Complex Fracturing ReseArch Code) + Mark McClure	THM	Continuum-Elastic + Discrete Fractures + Fracture Propagation + Stress Dependent Permeability	2D + Unstructured Mesh + Finite Volume Method + Implicit Temporal	Hydraulic fracturing and induced seismicity in complex fracture networks
FALCON (Fracturing And Liquid CONvection) + Robert Podgomey and Hai Huang	THMC	Continuum-Elastic + Continuum-Plastic + Discrete Fractures + Discrete Damage + Stress-Dependent Permeability +	3D + Structured Mesh + Unstructured Mesh + Adaptive Mesh + Finite Element + Implicit and Explicit Temporal	Geothermal + reactive flow and transport + repository design
FLAC3D + Lee Petersen	M + TH	Large-Strain Simulation of Continua + Slip Planes Simulating Faults, Joints or Frictional Boundaries + 3 Elastic Models + 8 Plasticity Models + Optional Thermal Creep + Optional Variably Saturated Flow through Geologic Media	3D + Explicit Finite Difference Formulation + Stable Solutions to Unstable Physical Processes + Automatic 3D Grid Generator	Advanced geotechnical analysis of soil, rock, and structural support in three dimensions
FEHM (Finite Element Heat and Mass) + George Zvyvoloski	THMC	Coupled Geomechanics (THM) Problems (Fluid Flow and Heat Transfer Coupled with Stress/Deformation) + Non-Linear Elastic and Plastic Deformation + Nonlinear Functional Dependence of Rock Properties (e.g. Permeability, Porosity, Young's Modulus) on Pressure, Temperature and Damage/Stress	3D + Finite Element Method + Control Volume Method + Unstructured Grids + Fully Implicit Temporal	Basin-scale groundwater systems, migration of environmental isotopes in the vadose zone, geologic carbon sequestration, oil shale extraction, geothermal energy, migration of nuclear and chemical contaminants, methane hydrate formation and formation of karst
GeoFrac-Mech	THM	Elastic fracture mechanics analysis of fractures and fracture networks + Thermo-poroelastic fracture mechanics analysis of fractures and fracture networks	2D Boundary Element Method	Fracture Mechanics in Geothermal and Petroleum Reservoir Engineering
GeoFrac-Stim	THM	2D and 3D Thermo-Poroelastic Fractured Reservoir Model (Injection/Extraction) + 3D Thermo-Poroelastic Reservoir Model with Stochastic Fracture Networks and Continuum Damage Mechanics	Boundary Element Method and Finite Element Method	Geothermal Reservoir Creation + Hydraulic Stimulation + Hydraulic Fracturing + Potential Occurrence of Micro Earth Quake

Table 2 continued

Code + developer(s)	Class type	Key capabilities	Spatial and temporal discretization	Primary application
GEOS + Randolph Settgast, Scott Johnson, Stuart Walsh, Pengcheng Fu et al.	THMCS	Continuum-Elastic + Continuum-Plastic + Fracture Propagation + Displacement-Based Governing Equations + Stress-Based Governing Equations + Stress-Dependent Permeability + Solute Transport + Precipitation/Dissolution	3D + Unstructured Mesh + Finite Element + Finite Volume + Discrete Element + Lagrangian Particle Tracing + Fully Implicit, Explicit and Euler Temporal	Hydraulic stimulation of fractured rock formations + long term production from fractured reservoirs
GPRS (General Purpose Reservoir Simulator) + Roland Horne and Yang Wong	TH	Two-Phase (Water-Air) + Three Phase (Water-Oil-Air) + Darcy Flow + Discrete Fracture Flow + Ideal Gas Law + Cubic Equation of State (Peng-Robinson)	3D + Structured Mesh + Unstructured Mesh + Finite Volume + Cartesian Coordinates + Fully Implicit Temporal	Multiphase, multi-component mass and energy flow
MULTIFLUX + George Danko, Davood Bahrami	THMC	Numerical Transport Code Functionalization (NTCF) + Direct Iteration and Successive Approximation Coupler (DISAC) + Inside Balance Iteration (IBI)	External or Internal Computational Fluid Dynamic Solver + External Porous-Media Hydrothermal Code (e.g., TOUGH2, NUFT) + External Rock Mechanics Code (e.g., 3DEC)	Enhanced Geothermal Systems + Mine Ventilation + Nuclear Waste Repository Ventilation
NUFT (Nonisothermal Unsaturated-saturated Flow and Transport) + John Nitao, Yue Hao, et al.	THC	Ideal Gas Law + Cubic Equation of State (Peng-Robinson) + Fundamental (Span-Wagner) Solute Transport + Single-Component Reactions + Multi-Component Reactions + Equilibrium Reactions + Kinetic Reactions + Precipitation/Dissolution + Porosity-Permeability Modification	3D + Structured Mesh + Unstructured Mesh + Finite Volume + Cartesian Coordinates + Cylindrical Coordinates + Fully Implicit Temporal	Subsurface flow and transport modeling
PELOTRAN (A Massively Parallel Reactive Flow and Transport Model for Describing Surface and Subsurface Processes) + Peter Litchner, Glenn Hammond et al.	THC	Richard's Equation + Multiphase Water-Supercritical CO ₂ + Surface Flow + Discrete Fracture Network + Aqueous Complexation + Sorption + Mineral Precipitation and Dissolution + Multiple Continuum for Heat + Subsurface Flow-Reactive Transport Coupling + Multiphase Ice-Water-Vapor Flow	3D + Structured Grid + Unstructured Grid + Finite Volume + Fully Implicit Backward Euler Temporal + Fully Implicit or Operator Splitting Reactive Transport	HPC Subsurface Flow and Reactive Transport + Hanford 300 Area + Copper Leaching + CO ₂ Sequestration + Multiple Continuum Model
STOMP (Subsurface Transport Over Multiple Phases) + Mark White and Diana Bacon	THMC	Coupled Flow and Transport + Sequential Geochemistry and Geomechanics + Stress Dependent Permeability + Continuum-Elastic + Equilibrium, Conservation, and Kinetic Reactions + Precipitation/Dissolution	3D Structured + Finite Volume Method + Implicit Temporal	Modeling of multifluid flow, heat transfer, and geochemistry in geologic media
TOUGH2 (Transport Of Unsaturated Groundwater and Heat) + Karsten Pruess	TH	Different Fluid Mixtures + Properties Described in Equation-of-State (EOS) Modules + Thermophysical Properties of Water by Steam Table Formulations + Double-Porosity, Dual-Permeability and Multiple Interacting Continua (MINC) methods	3D + Integral Finite Difference Spatial + First-Order Fully Implicit Temporal	Nonisothermal multiphase flow in fractured porous media, primarily designed for geothermal reservoirs and high-level nuclear waste isolation

Table 2 continued

Code + developer(s)	Class type	Key capabilities	Spatial and temporal discretization	Primary application
TOUGHREACT (Transport Of Unsaturated Groundwater and Heat) + Karsten Pruess	THC	TOUGH2 + Precipitation/ Dissolution + Modification of Porosity, Permeability, and Unsaturated Characteristics + Mass Conservation Written in Terms of Basis (Component) Species + General Rate Law for Kinetically Controlled Mineral Dissolution and Precipitation Reactions	3D + Integral Finite Difference Spatial + First-Order Fully Implicit Temporal	Reactive chemistry with interactions between mineral assemblages and fluids under local equilibrium or kinetic rates, and chemically active gas phase

Class type key: *T* thermal energy transport, *H* hydrologic mass transport, *M* geomechanics, *C* geochemistry, *S* seismic wave propagation

demonstration site in southern Idaho (Bradford et al. 2013; Bradford et al. 2015; Huang et al. 2013). However, the data were simplified and generalized for the purposes of the code comparison study. The simulation problem involved a poroelastic fault layer in a geothermal reservoir undergoing water injection. The observed reservoir behavior includes a strong non-linear response between the injection rates and pressures over multiple-day, variable-rate injection tests. Water injected into a fracture within a geothermal reservoir alters the effective stress within the fracture by altering the fluid pressure and formation temperature. This problem considers changes in fracture permeability and injection pressure in response to changes in the effective stress within the fracture, and is based on field observations (Nathenson 1999). In this problem water is injected from a vertical well into a horizontal fracture zone with a uniform thickness of 4 m at a depth of 2000 m below ground surface. Water is injected at a constant rate of 80 kg/s at a temperature of 140 °C, which is equivalent to the formation temperature, thus eliminating the thermal stress component. The computational domain extends horizontally 2000 m (i.e., 2828.4 m radially) from the center of the well. Constant pressure conditions are specified at the outer radial distance equivalent to the initial pressure of 20 MPa. Two scenarios are considered: (1) no-leak-off and (2) leak-off. In the no-leak-off scenario, the reservoir formation outside of the fracture (i.e., basalt) is assumed to have near zero permeability and in the leak-off scenario the basalt formation has finite permeability. Problem specifications are provided in Sect. 5 of White et al. (2016b).

Eleven teams submitted results for this problem as listed in Table 4. The constant injection rate formulation of this problem leads to a similitude solution during the transient stage of the simulation. Increases in pore pressure decrease the effective stress, leading to an increase in fracture permeability. Simulation results during the transient stage were dependent on the fracture compressibility and basalt formation permeability. The leak-off scenario yielded lower injection pressures and increases in fracture permeability, as injected fluid was lost into the basalt. The original formulation of this problem included a thermal stress component that was effected by injecting cold water into the fracture. The problem was altered to its isothermal form to aid in the initial round of code comparisons. Saturated water equilibrium

Table 3 Processes included in the benchmark problems

Processes	Prb. 1	Prb. 2	Prb. 3	Prb. 4	Prb. 5	Prb. 6	Prb. 7
Flow in porous media	*					*	
Flow in fracture zone	*	*			*		
Flow in discrete fracture			*	*		*	*
Poromechanics		*				*	
Mechanics of discrete fracture			*	*		*	*
Heat transport				*	*	*	
Thermal stress				*		*	
Geochemistry					*		

pressure at 140 °C is 0.3613 MPa, so the reservoir fluid remains in liquid form (i.e., no flash calculations are required for this problem). Submitted problem solutions are provided in Sect. 5 of White et al. (2016b). Example submittals for pressure versus time and pressure versus distance for the no-leak-off scenario are shown in Figs. 1 and 2, respectively.

3.2 Benchmark problem 2: shear stimulation of randomly oriented fractures via pore pressure increase and thermal stress

3.2.1 Problem champion: Sharad Kelkar, Los Alamos National Laboratory

Benchmark Problem 2 was motivated by the shear stimulation treatment of Well 27-15 at the Desert Peak geothermal field in September 2010 (Chabora et al. 2012) and the subsequent modeling analysis (Dempsey et al. 2013). Observed results of the field stimulation including injection rate, wellhead pressure (WHP) and downhole pressure (DHP) are shown in Fig. 3. Water at 100 °C is injected at a specified pressure over a period of 27 days into a three-dimensional fractured reservoir via a well with a flowing surface area of 1.131 m². The initial reservoir temperature was a uniform 190 °C and the initial fluid pressure in the reservoir at the injection horizon was 9.81 MPa. The problem domain was specified to extend horizontally to 200 m (282.4 m radially) from the injection point. Fluid pressure at the external boundaries was specified as being equal to the initial pressure and the external boundaries were considered to be adiabatic for heat flow. The problem specification used a Cartesian grid for orientation, taking advantage of the 1/8 symmetry, with the injection point being located at the coordinate system origin

(i.e., x, y, z = 0, 0, 0). The downward vertical (i.e., negative z-direction) mechanical stress was 22.7 MPa, the minimum horizontal stress, applied at the external boundary in the x-direction was 13.88 MPa, and the maximum horizontal stress, applied at the external boundary in the z-direction was 18.3 MPa.

Fluid flow in the reservoir was assumed to occur through randomly oriented fractures, with an isotropic intrinsic permeability that was a function of a Mohr–Coulomb stress, which was defined as a function of the local maximum and minimum principal stresses, the local fluid pressure, and a constant coefficient of friction and cohesion. The primary objective of the simulation problem was to predict the injection rate as a function of time. Coupled hydrological, thermal, and geomechanical processes were to be considered:

- single-phase fluid mass balance with Darcy’s law governing fluid flow
- thermal energy balance including advection and conduction
- static force balance with linear poro-elasticity (Biot’s theory) and thermal stress
- the Mohr–Coulomb criteria for shear failure using effective stress:

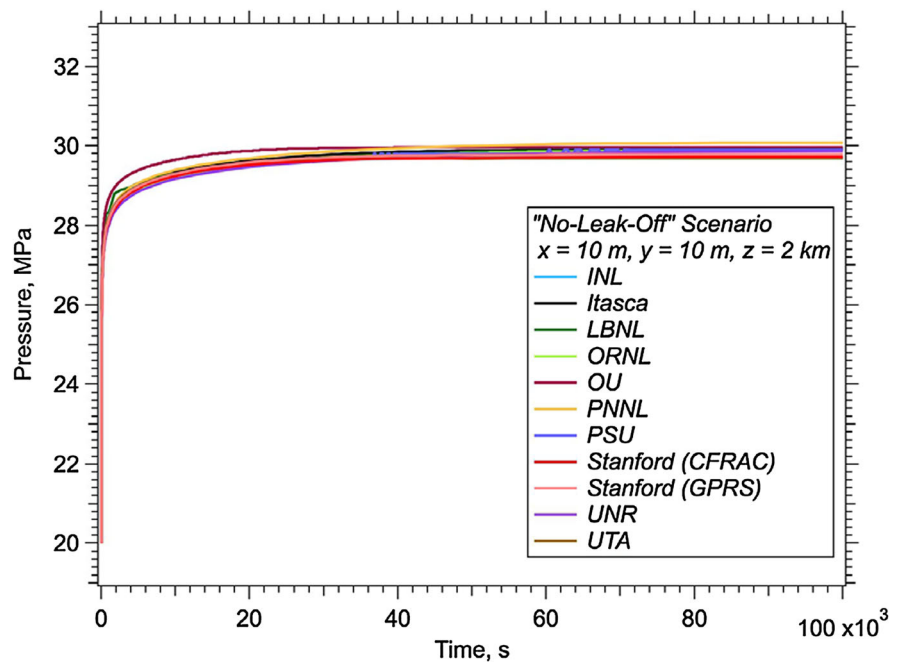
$$MC_{stress} = \frac{1}{2}(\sigma_1 + \sigma_3)(\mu^2 + 1)^{\frac{1}{2}} - \frac{1}{2}\mu(\sigma_1 + \sigma_3) + \mu P - S_0 \tag{1}$$

- where MC_{stress} is the Mohr–Coulomb stress, σ_1 and σ_3 are the local maximum and minimum principal stresses, P is the pore pressure, μ is the coefficient of friction, and S_0 is the cohesion
- permeability enhancement as a specified function of the Mohr–Coulomb stress upon reaching the failure criteria:

Table 4 Participating teams and computer codes for benchmark problem 1

Simulation team	Code(s)
Idaho National Laboratory (INL)	FALCON
Itasca Consulting Group (Itasca)	FLAC ^{3D}
Lawrence Berkeley National Laboratory (LBNL)	TOUGH and FLAC ^{3D}
Lawrence Livermore National Laboratory (LLNL)	GEOS
Oak Ridge National Laboratory (ORNL)	PFLOTRAN
Pennsylvania State University (PSU)	FLAC3D and TOUGHREACT
Pacific Northwest National Laboratory (PNNL)	STOMP
Stanford University (Stanford)	CFRAC and AD-GPRS
University of Nevada, Reno (UNR)	MULTIFLUX and TOUGH2
The University of Oklahoma (OU)	GEOFRAC
The University of Texas at Austin (UTA)	CFRAC-UT

Fig. 1 Pressure solution versus time at $r = 14.142$ m for the “no-leak-off” scenario



$$\begin{aligned}
 K &= K_{initial} \text{ if } MC_{stress} < 0 \\
 K &= K_{initial} + \left(\frac{MC_{stress}}{MC_{ramp}} \right) (K_{max} - K_{initial}) \\
 &\quad \text{if } 0 \leq MC_{stress} \leq MC_{ramp} \\
 K &= K_{max} \text{ if } MC_{stress} > MC_{ramp}
 \end{aligned}
 \tag{2}$$

where $K_{initial}$ is the initial permeability, K_{max} is the maximum allowed permeability, and MC_{ramp} is the ramp stress (i.e., range of MC_{stress} over which the permeability ramps from the initial to maximum value).

The simulation duration was 27 days. Problem specifications are provided in Sect. 6 of White et al. (2016b).

Eight teams participated in the solutions using various simplifying assumptions, multiple runs and THM models as listed in Table 5. Metrics for this problem were the injection rate versus time, and temperature, pressure, and the defined Mohr–Coulomb stress at two distances from the injection point (i.e., $x = y = z = 2.5$ m or $r = 4.33$ m and $x = y = z = 7.5$ m or $r = 13.0$ m). The original problem specifications include grid dimensioning,

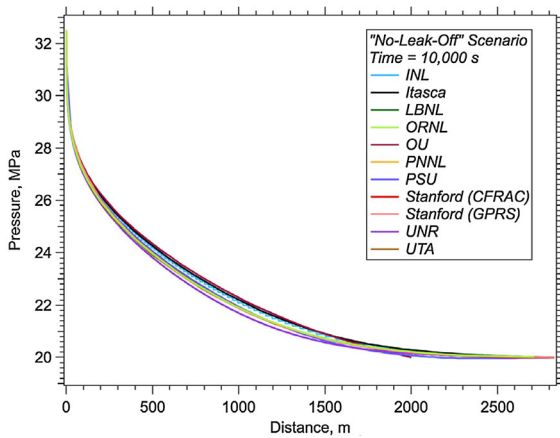
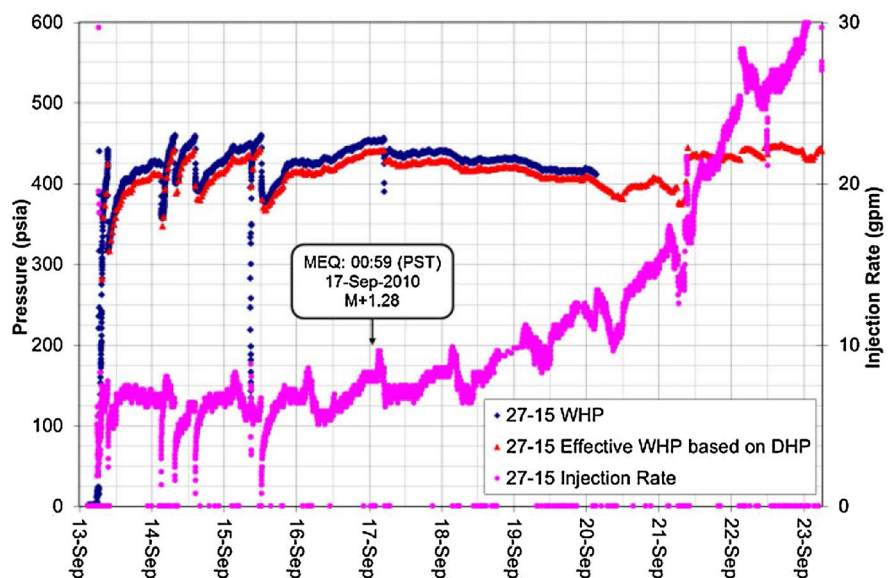


Fig. 2 Pressure solution versus distance at $t = 10^4$ s for the “no-leak-off” scenario

but no reference to an injection surface area. Preliminary results for this problem, conducted by the LBNL team, indicated a strong sensitivity to spatial discretization and the surface area for the well. After the LBNL analysis of the problem, teams were advised to conduct independent grid convergence analysis and the well surface area was specified. Agreement of results between teams for this problem was scattered, with like modeling approaches and grid discretization yielding acceptable agreement in injection rate and temperature, pressure, and displacement at the nearest

Fig. 3 Observed results of the field stimulation at Desert Peak Well 2715



metric point, but poorer agreement for the second metric point away from the well. Saturated water equilibrium pressure at 190 °C is 1.254 MPa, so the reservoir fluid remains in liquid form (i.e., no flash calculations are required for this problem).

The injection flow rates, scaled by a factor of 8 for the entire spherical domain, as a function of time for the various models are plotted in Fig. 4. Also, shown in this figure are the two bounding curves calculated using the LANL model shown by dashed grey lines for constant permeabilities with the high (143 mD) and low (2.6 mD) values—these can be expected to be the high and low bounds on the flow rates. In the case of constant formation permeability, the injection rate at a constant injection pressure is seen to decrease with time as expected. However, in this problem the permeability is a function of the MC_{stress} , and increases with time due to pore pressure and temperature changes as demonstrated in Fig. 5. This causes the flow rate to increase with time. The increase is rapid at the start and slows down as time progresses as can be seen in Fig. 4. The predicted injection rates after 25 days fall in the interval of 3.6–5.8 kg/s, with the PSU model predicting the lowest and the LBNL predicting the highest values. Experimental injection rates, shown in Fig. 3, refer to conditions at the ground surface.

Table 5 Participating teams and computer codes for benchmark Problem 2

Simulation team	Code(s)
Idaho National Laboratory (INL)	FALCON
Itasca Consulting Group (Itasca)	FLAC ^{3D}
Lawrence Berkeley National Laboratory (LBNL)	TOUGH and FLAC ^{3D}
Los Alamos National Laboratory (LANL)	FEHM
Pacific Northwest National Laboratory (PNNL)	STOMP
Pennsylvania State University (PSU)	FLAC3D and TOUGHREACT
Stanford University (Stanford)	CFRAC and AD-GPRS
The University of Oklahoma (OU)	GEOFRAC
The University of Texas at Austin (UTA)	CFRAC-UT

3.3 Benchmark problem 3: fracture opening and sliding in response to fluid injection

3.3.1 Problem champion: Mark McClure, The University of Texas at Austin

This isothermal problem, based on based on simulations performed by McClure (2012) and Mutlu and Pollard (2008), involves the injection of fluid under into three horizontally connected fractures of finite length, as shown in Fig. 6. The first fracture is oriented parallel to the maximum principal stress of $\sigma_{yy} = 26$ MPa and perpendicular to the minimum principal stress of $\sigma_{xx} = 21$ MPa and has a length of 17 m. The second (central) fracture is joined to the end of the first fracture and is oriented at angle of 30.465° to the maximum principal stress and has a length of 39.446 m. The third fracture is joined to the end of the second, oriented parallel to the maximum principal stress, and has a length of 17 m. Fluid is injected into the center of the second (central) fracture at a constant pressure of 20.25 MPa, where the initial fluid pressure was 18 MPa. No fluid was allowed to leak from the fractures. The interesting element of this problem is that the injection pressure was selected to be the normal stress on the fracture at all times and for all fracture elements (i.e., $\sigma_{normal} = 21$ MPa for the first and third fractures, and $\sigma_{normal} = 22.29$ MPa for the second (central) fractures. At the injection pressure, however, the shear stress on the central fracture (i.e., $\sigma_{shear} = 2.186$ MPa) is sufficient to cause slip along the fracture, yielding fracture opening near the first–second fracture joint and second-third fracture joint. Problem specifications are provided in Sect. 7 of White et al. (2016b).

The geometry of the 3-fracture system is shown in Fig. 6. For the flow calculations, an out-of-plane thickness, $h = 100$ m, for the fractures is assumed (so that the elements do not have infinite volume). Simplifying assumptions are:

- isothermal conditions
- single-phase, single-component fluid
- constant fluid viscosity
- constant fluid compressibility
- no leakoff from the fractures
- constant fracture transmissivity, including for open fractures (i.e., walls out of contact)
- no chemical effects
- stress induced by slight normal displacement of closed fracture elements are neglected

The fractures are assumed to have a constant compressibility so that the fracture aperture of a closed element can be given by the simple equation:

$$E = E_{ref} \exp(c_E [\sigma_n - P]) \quad (3)$$

where E is aperture (i.e., volume of fluid stored per surface area of fracture), σ_n is normal stress, c_E is the fracture compressibility, and P is the fluid pressure. For an open fracture element, the aperture is given by the equation:

$$E = E_{ref} + E_{open} \quad (4)$$

where E_{open} is the mechanical opening of the fracture. Because the fracture transmissivity is assumed constant, the hydraulic aperture is effectively assumed to be constant. Although constant fracture transmissivity is not realistic, this assumption was made in order to simplify the problem and facilitate comparison between codes.

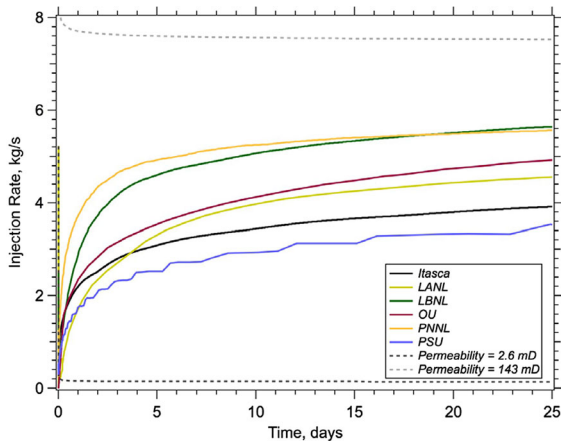


Fig. 4 Simulation results for injection rate versus time

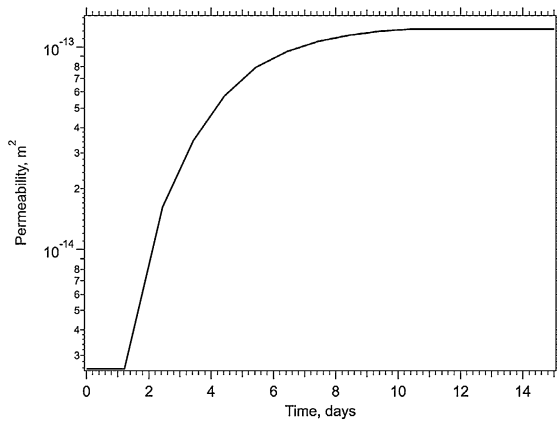


Fig. 5 Permeability calculated by LANL at 4.33 m from the injection point as a function of time

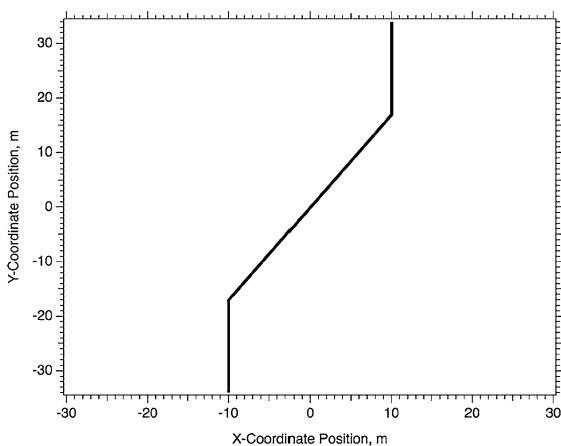


Fig. 6 Problem geometry with three pre-existing fractures

Seven teams submitted results for this problem as listed in Table 6. Fracture opening and slip occurred in response to the fluid injection. Fracture opening occurred via two mechanisms: (1) increase in fluid pressure and (2) shear along the central fracture, yielding fracture opening in the first and third fractures. Fracture opening purely due to the increase in fluid pressure was generally small (i.e., 0.022 mm) at equilibrium, however, maximum fracture openings in the first and third fractures near the joints with the second fracture due to slip along the second (central) fracture were more than 30 times that purely due to the increase in fluid pressure. Agreement between the teams for the fracture opening and slip profiles along the length of the fractures was good at equilibrium. More variance was noted during the transient stage of the problem, both in terms of the injection rate and fracture opening and slip profiles. A temperature was not specified for the problem, but the fluid in the fractures is assumed to remain in liquid form with a density of 1000 kg/m³.

As seen in Fig. 7, the injection rate is highest at the beginning of the simulation and gradually declines to zero over time. At the start of the simulation, there is a sharp pressure difference between the well (which injects at a constant pressure) and the adjacent fracture. Because there is no leakoff into the matrix, the fluid pressure eventually rises to equal the injection pressure everywhere, and the injection rate goes to zero. The PSU and LBNL results have a lower rate than the other simulation results at all times, suggesting that there is less cumulative fluid injection in these simulations than in the others, probably caused by differences in how fluid storage is calculated. Both UNR results deviate significantly from the general trend of the other results. The Itasca result has one of the lowest injection rates at early time, and the highest rate at late time, suggesting that a similar cumulative volume of fluid is injected, but there is some difference in the way fracture transmissivity is calculated. The OU result deviates significantly from the other results during the first 100 s, before settling onto a very similar trend. This is probably because the OU result started the simulation with comparatively large time steps (around 30 s).

The aperture results after 60 s of injection are quite variable (Fig. 8). These results are affected by the time-dependent process of fluid pressure spreading through the fractures. At 60 s, the region where significant aperture change occurs is small, and the gradient in

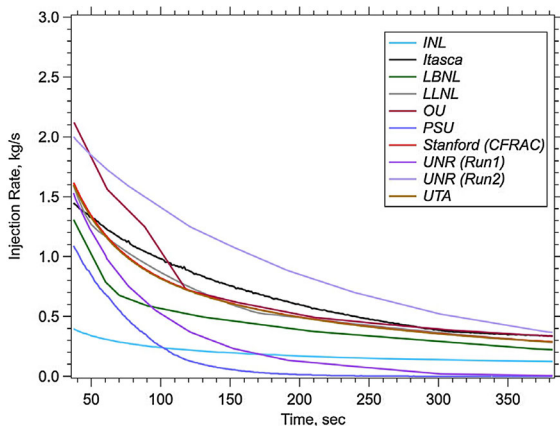


Fig. 7 Simulation results for injection rate versus time

aperture is significant. Some of the simulations are not performed with adequate mesh refinement to capture this behavior in detail. The PSU result has more opening along the peripheral fractures than the other results. The UNR Run 2 result matches several other simulations in maximum opening near the juncture, but predicts significantly more opening along the length of the peripheral fractures. As with the other results for Benchmark Problem 3, the Stanford and UTA results are nearly identical, with the Stanford curve overlaying and obscuring the UTA result on the figure.

3.4 Benchmark problem 4: planar EGS fracture of constant, penny-shaped aperture in permeable hot rock

3.4.1 Problem champion: George Danko, University of Nevada at Reno

The fourth problem was motivated by the first experimental EGS in the U.S. at Fenton Hill (Murphy

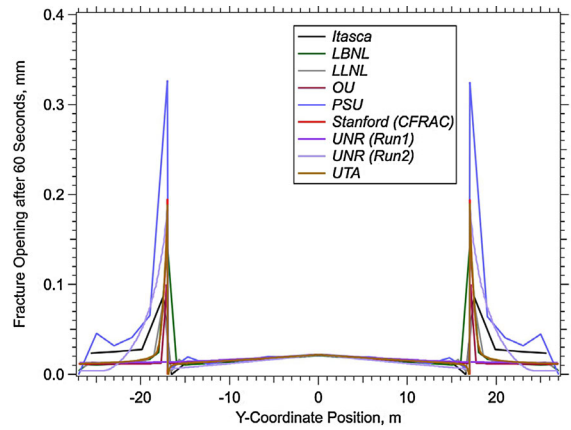


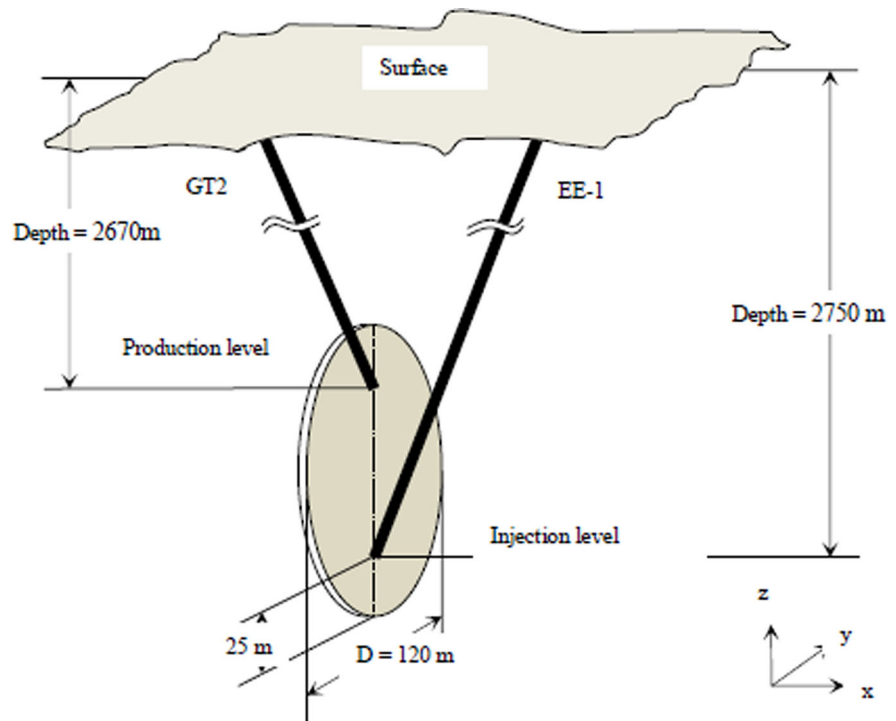
Fig. 8 Simulation results for change in fracture aperture (i.e., from the initial aperture) after 60 s of injection

et al. 1981) and involves a single planar fracture oriented vertically with two slanted wells that intersect the fracture. The injection well intersects the fracture at 2750 m bgs and the production well intersects the fracture at 2630 m bgs. The fracture has a diameter of 120 m, with the bottom of the fracture being at 2770 m bgs. These arrangement is an idealization of the configuration at Fenton Hill, as shown in Fig. 9. Two scenarios are considered for this problem: (1) constant aperture, penny-shaped fracture, and (2) variable aperture, lens-shaped fracture. In the first scenario water flows from the injection well to the production well via a constant aperture fracture equal to 0.141 mm. In the second scenario, the fracture aperture varies with the elastic and thermal dilatation of the rock, starting with an initial aperture of $1.e-6$ m. The rock temperature at 2750 m bgs was 185 °C. A geothermal gradient of 100 °C/km was assumed to 2300 m bgs, and then transitions to 55 °C/km to the ground surface. Water is injected at a

Table 6 Participating teams and computer codes for benchmark Problem 3

Simulation team	Code(s)
Idaho National Laboratory (INL)	FALCON
Itasca Consulting Group (Itasca)	FLAC ^{3D}
Lawrence Berkeley National Laboratory (LBNL)	TOUGH and FLAC ^{3D}
Lawrence Livermore National Laboratory (LLNL)	GEOS
Pennsylvania State University (PSU)	FLAC3D and TOUGHREACT
Stanford University (Stanford)	CFRAC and AD-GPRS
University of Nevada, Reno (UNR)	MULTIFLUX and TOUGH2
The University of Oklahoma (OU)	GEOFRAC
The University of Texas at Austin (UTA)	CFRAC-UT

Fig. 9 Simplified reservoir geometry (after (Murphy et al. 1981))



constant rate of 7.5 kg/s for the first 24 days and then at 15.0 kg/s between 24 and 75 days. The injection temperature was specified via tabular input as a function of time, designed to be in agreement with a constant surface temperature of 25 °C. Rock matrix properties were isotropic-homogeneous and based on data from Fenton Hill (Murphy et al. 1981). To more accurately model the Fenton Hill field test, outlet pressures were specified as a function of time. Problem specifications are provided in Section 8 of White et al. (2016b).

A penny-shaped, planar fracture (constant aperture) is defined with impermeable rock around it following as closely as possible the EGS arrangement at the Fenton Hill Phase I experiments. The key assumption is that the geometry of the planar fracture is known with a given constant fracture aperture, and a given constant radial extension in the plane. Note that an open fracture and not a porous layer are defined.

In the second scenario, the radial extension of the planar fracture is constant as in the first, however, the aperture of fracture is assumed to change due to the elasticity and thermal dilatation of the rock. A simple, linear thermo-mechanical, elastic fracture aperture model may be used by calibration to the in situ

measurement results as follows (Danko and Bahrami 2013a, b):

$$\delta(x, y) = \delta_0 + C_P [P(x, y) - P_0(x, y)] + C_T \Delta L [T(x, y) - T_0(x, y)] \quad (5)$$

where δ is the hydrodynamic fracture aperture, δ_0 is the initial fracture aperture, C_P is the pressure aperture coefficient, C_T is the thermal aperture coefficient, P_0 and T_0 are the initial pressure and temperature, P and T are the pressure and temperature, and ΔL is the thermal contraction. However, other joint characteristics are used by some project participants. The LLNL model applies the Barton-Bandis exponential joint characteristics, while the UTA model uses the in situ stress as a threshold pressure for the unconfined fracture opening. The properties and the in situ virgin temperature of the rock are also known. The injection flow rate and temperature as a function of time likewise follow given trends from published data (Murphy et al. 1981). The injection and production boreholes are assumed to be heated and/or cooled by the surrounding rock mass during circulation.

Six teams submitted results for constant aperture scenario and four teams submitted results for the penny-shaped (i.e., variable aperture) scenario, as listed in Table 7. Pressure results for the constant aperture

Table 7 Participating teams and computer codes for benchmark Problem 4

Simulation team	Code(s)
Itasca Consulting Group (Itasca)	FLAC ^{3D}
Lawrence Berkeley National Laboratory (LBNL)	TOUGH and FLAC ^{3D}
Lawrence Livermore National Laboratory (LLNL)	GEOS
University of Nevada, Reno (UNR)	MULTIFLUX and TOUGH2
The University of Texas at Austin (UTA)	CFRAC-UT

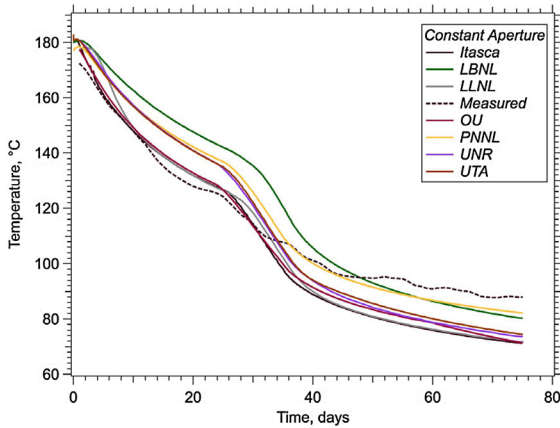


Fig. 10 Simulation results for temperature versus time for the constant aperture scenario

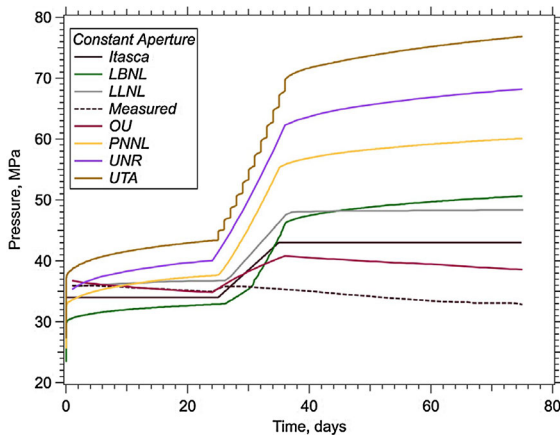


Fig. 11 Simulation results for pressure versus time for the constant aperture scenario

scenario show similar trends between the submitted results, but additionally show scatter between the teams; moreover, the pressure results do not match the trends observed at Fenton Hill. At Fenton Hill pressures increased sharply with jumps in the inject rate, but then decayed over time with constant injection. Submitted simulation results for temperature showed generally

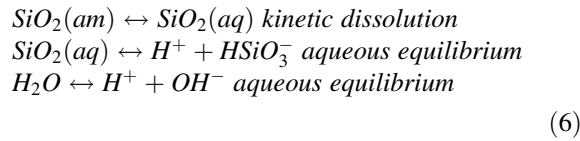
good agreement among the teams and reasonable agreement with the outlet temperature history observed at Fenton Hill. As the injection rate is specified for this problem the agreement between simulation results in terms of temperature indicates all of the simulators are modeling fluid enthalpy and heat transfer processes correctly, as shown in Fig. 10, for the constant aperture scenario. Data from Fenton Hill is noted as “Measured.” All models over-predict the extraction temperature significantly and thus the available heat extraction potential; and all under-predict the thermal drawdown. Pressure results for the variable aperture scenario had considerable scatter between simulation results, but results from two teams did yield declining pressures, following sharp pressure increases with jumps in the injection rate, as shown in Fig. 11, for the constant aperture scenario. Data from Fenton Hill is noted as “Measured.” The upward trend in pressure change with time for a constant injection flow rate from the constant-aperture models is opposite from the measured trend of pressure variation, a proof for fracture aperture opening with time. This opposite trend clearly implies the need for modeling fracture opening due to thermal drawdown through thermo-mechanical coupling.

3.5 Benchmark problem 5: amorphous silica dissolution/precipitation in a fracture zone

3.5.1 Problem champion: Mark White, Pacific Northwest National Laboratory

Flow of water through an idealized horizontal fracture zone is considered with temperature dependent reaction of the water with a formation mineral. This problem is an altered version of the simulations conducted by Xu and Pruess (Xu et al. 2004) that investigated the effects of mineral scaling and clay swelling in a fractured geothermal reservoir. The chemical reaction network for this problem was reduced from the (Xu and Pruess 2004) configuration

to a single dissolving mineral, yielding a network of three reactions:



Although the number of chemical species was reduced the problem retained the challenges of having the kinetic amorphous silica dissolution reaction having temperature dependence in both the kinetic rate and equilibrium constants, following the general form of the rate law (Steeffel and Lasaga 1994). The fracture zone comprises three regions: (1) fracture, (2) altered granite, and (3) unaltered granite. The flow of water is predominately through the fracture, but the altered granite and unaltered granite have finite intrinsic permeability and porosity. Water at 65 °C is injected into the fracture zone, which is initially at 200 °C. The dissolution and precipitation of amorphous silica along the length of the fracture zone is to be computed for two forms of injected water: (1) pure water and (2) recycled water. Changes in intrinsic permeability and porosity due to mineral dissolution and precipitation are also considered. A relationship between changes in porosity and intrinsic permeability developed by Verma and Pruess (1988) is used to more accurately capture effect of pore-throat clogging by precipitates. Metrics for this problem were profiles of temperature, pressure, porosity, and permeability within the fracture across the domain at 10 years; aqueous concentrations of H⁺, OH⁻, HSiO₂⁻, and SiO₂ (aq) as a function of time at 3.0 m from the inlet; and change in amorphous silica abundance as a function of time at 3.0 m from the inlet. Problem specifications are provided in Section 9 of White et al. (2016b).

The Verma and Pruess (1988) model was used to relate changes in porosity with changes in intrinsic permeability; where, the critical porosity was defined

as 80% of the initial porosity and the functional exponent was 2:

$$\frac{k}{k_0} = \left(\frac{\phi - \phi_c}{\phi_0 - \phi_c} \right)^n; \quad \phi_c = 0.8; \quad n = 2 \tag{7}$$

where k is intrinsic permeability, m^2 , k_0 is the reference intrinsic permeability, m^2 , ϕ is the porosity, ϕ_c is the critical porosity, ϕ_0 is the reference porosity, and n is the functional exponent.

As shown in Eq. (6), the reaction network comprises one kinetic reaction for the dissolution of $SiO_2(am)$ and two equilibrium reactions between the aqueous species. For the equilibrium reaction, the equilibrium constants were assumed to be a function of temperature:

$$\log K = c_1 \ln(T) + c_2 + c_3 T + \frac{c_4}{T} + \frac{c_5}{T^2}; \tag{7}$$

with T in °K

where the coefficients for the two equilibrium reactions are shown in Table 8. The kinetic reaction rate is expressed in terms of the change in amorphous silica per time, mol/s, using a common form for kinetic mineral dissolution and precipitation (Steeffel and Lasaga 1994):

$$\frac{\partial SiO_2(am)}{\partial t} = k_{25} A_m \left[1 - \frac{Q_m}{K_m} \right] \exp \left[\frac{-E_a}{R} \left(\frac{1}{T} - \frac{1}{T_{25}} \right) \right]; \tag{8}$$

with T in °K

where $SiO_2(am)$ are the moles of amorphous silica, k_{25} is the reaction rate at 25 °C, mol/m² s, A_m is the specific mineral surface area, cm²/g, Q_m is the ion activity product, K_m is the equilibrium constant, E_a is the activation energy, kJ/mol, R is the ideal gas constant (8.314 J/K mol), T is the temperature, °K and T_{25} is the reference temperature (298.15 °K). The parameters for this equation (Eq. 8) are shown in Table 9.

Table 8 Equilibrium reactions and coefficients for the temperature-dependent equilibrium constant

Equation	c_1	c_2	c_3	c_4	c_5
$H_2O \leftrightarrow H^+ + OH^-$	1.167×10^2	-7.455×10^2	-1.170×10^{-1}	3.916×10^4	-2.637×10^6
$SiO_2(aq) \leftrightarrow H^+ + HSiO_3^-$	5.733×10^0	-1.374×10^1	-3.538×10^{-2}	-8.173×10^3	8.088×10^5

Table 9 Kinetic reactions, parameters, and coefficients for the temperature-dependent equilibrium constant

k_{25} (mol/m ² s)	E_a (kJ/mol)	A_m (cm ² /g)	c_1	c_2	c_3	c_4	c_5
3.8×10^{-10}	49.8	9.8	1.014×10^2	-6.658×10^2	-7.844×10^{-2}	4.266×10^4	-3.055×10^6

The kinetic reaction rate, shown in Eq. (8), depends on the ratio of the ion activity product to the equilibrium product. The greater the difference in these two parameters the greater the departure from equilibrium and the faster the reaction rate. For a general kinetic reaction where species *A* and *B* react to produce *C* and *D*:



where *a*, *b*, *c*, and *d* represent the number of moles of these constituents. At chemical equilibrium, the distribution of chemical species mass between reactants and products can be expressed as:

$$K_m = \frac{[C_{eq}]^c [D_{eq}]^d}{[A_{eq}]^a [B_{eq}]^b} \quad (10)$$

where $[A_{eq}]$, $[B_{eq}]$, $[C_{eq}]$, and $[D_{eq}]$ are the activities for the reactants and products at equilibrium. The ion activity product is computed in the same fashion as the equilibrium constant:

$$Q_m = \frac{[C]^c [D]^d}{[A]^a [B]^b} \quad (11)$$

If $Q_m/K_m > 1$, then the reaction tends toward the reactants (i.e., precipitation of $SiO_2(am)$ for Eq. 8), and conversely if $Q_m/K_m < 1$ then the reaction tends toward the products (i.e., dissolution of $SiO_2(am)$ for Eq. 8).

Species activity is computed from the product of the species concentration times its activity coefficient. Activity coefficients were calculated using the B-dot model, which is an extension of the Debye–Huckel model, with temperature dependent coefficients. There are two equations for computing the activity coefficient as a function of temperature and ionic strength, one for charged species and a second for neutral or nonpolar species. As the kinetic reaction for this problem only involves the dissolution of amorphous silica, without changes in associated charge the second form of the equation is used:

$$\log \gamma_o = aI + bI^2 + cI^3$$

$$a = \sum_{i=0}^3 c_a^i T^i (^\circ C) \quad b = \sum_{i=0}^3 c_b^i T^i (^\circ C)$$

$$c = \sum_{i=0}^3 c_c^i T^i (^\circ C)$$

$$c_a^0 = 1.31678 \times 10^{-1} \quad c_b^0 = -1.86731 \times 10^{-2}$$

$$c_c^0 = 2.88841 \times 10^{-3}$$

$$c_a^1 = -8.36829 \times 10^{-4} \quad c_b^1 = 3.9022 \times 10^{-4}$$

$$c_c^1 = -6.70405 \times 10^{-5}$$

$$c_a^2 = 3.07179 \times 10^{-6} \quad c_b^2 = -2.62611 \times 10^{-6}$$

$$c_c^2 = 5.65666 \times 10^{-7}$$

$$c_a^3 = 1.46701 \times 10^{-9} \quad c_b^3 = 4.40918 \times 10^{-9}$$

$$c_c^3 = -1.34012 \times 10^{-9}$$

Three teams submitted results for this geochemical problem, as listed in Table 10. For the fresh water scenario simulation results showed general agreement in the temperature, pressure, porosity, and permeability profiles at 10 years, as shown in Fig. 12 for temperature. The pressure profile showed a nearly linear decay, with a slower decay rate near the inlet, due to the dissolution of amorphous silica. Sharp decreases in porosity and permeability were additional noted in all the simulation results near the inlet, indicating the inlet water was saturated with aqueous species at the outlet, as shown in Fig. 13. For the recycle-water scenario, the problem is designed to have supersaturated conditions for dissolved aqueous species at the inlet. This results in precipitation of amorphous silica near the inlet. All the simulation results show decreases in porosity and permeability near the inlet for this scenario after 10 years, indicating precipitation of amorphous silica. Comparison of the aqueous species concentrations and change in amorphous silica abundance at 3.0 m from the inlet between the submitted simulation results agree with

the changes in porosity and permeability, indicating proper modeling of the equilibrium reactions.

3.6 Benchmark problem 6: injection into a fault/fracture in thermo-poroelastic rock

3.6.1 Problem champion: Ahmad Ghassemi, The University of Oklahoma

The principal objective of this problem is to illustrate the role of coupled thermo-poroelastic processes on natural fracture opening and shear deformation, which develops upon water injection into the fracture. The problem is two-dimensional and considers a 40-m long fracture oriented at 45° to the principal horizontal stress directions; where, the minimum principal stress is 13 MPa and the maximum principal stress is 20 MPa, as shown in Fig. 14. The original problem

specified an initial pore pressure, which was not in equilibrium with the mechanical stress state. The final form of the problem starts under equilibrium conditions with the principal stresses, initial pore pressure of 10 MPa, and temperature with an aperture of 1 mm. Water at 420° (isothermal) or 400 °K (nonisothermal) is injected into a reservoir at 420 °K at a constant rate of $0.6 \times 10^{-7} \text{ m}^3/\text{m}$ thickness of reservoir. The rock matrix properties are modeled after a Westerly granite. The problem is designed such that water injection into the fracture yields opening and shear. The shear strength of the fracture is modeled using the Bandis-Barton model (Bandis et al. 1983; Barton et al. 1985). The fracture normal stiffness is modeled following the Bandis (Bandis et al. 1983) joint closure function with a specified joint normal stiffness of 0.5 GPa/m and maximum joint closure of 3.0 mm. Metrics for the problem include reporting of the fluid pressure, fracture aperture, and fracture shear as a function of time; and profiles of fracture aperture and shear along the fracture length at 5, 75, and 180 days after the start of water injection.

The initial pore pressure is 10 MPa and the rock/fracture system is at a temperature of 420 K. The joint is in equilibrium with the prescribed stress and pore pressure and temperature conditions, and has an aperture of 0.5623 mm. This is the actual joint aperture under reservoir conditions and is calculated internally using the prescribed initial stiffness and

Table 10 Participating teams and computer codes for benchmark Problem 5

Simulation team	Code(s)
Lawrence Berkeley National Laboratory (LBNL)	TOUGH and FLAC ^{3D}
Lawrence Livermore National Laboratory (LLNL)	GEOS
Pacific Northwest National Laboratory (PNNL)	STOMP

Fig. 12 Temperature and pressure solutions for the “pure” water scenario

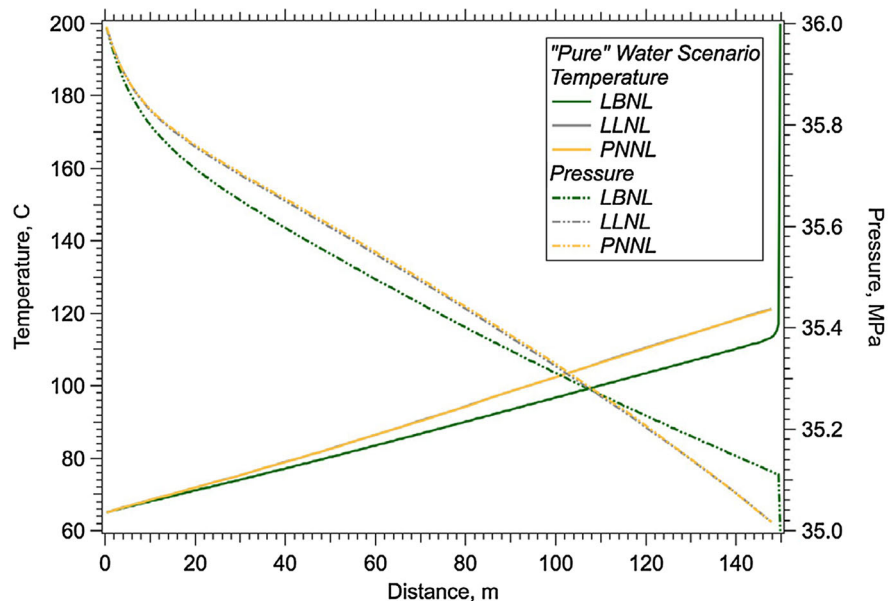
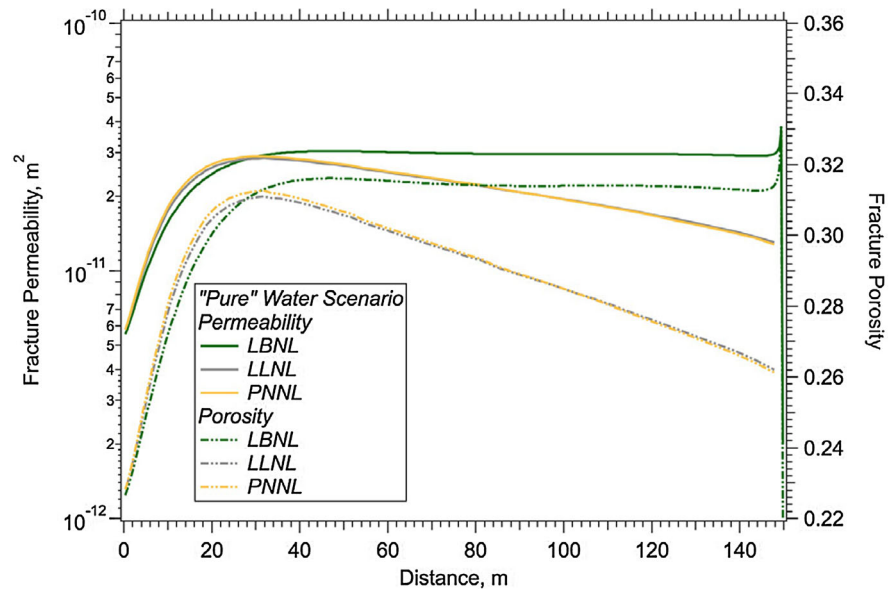


Fig. 13 Permeability and porosity solutions for the “pure” water scenario



stress state. The maximum joint closure is 3 mm. Liquid viscosity of the injected fluid is chosen to be at the average system temperature. To isolate the impact of thermal stresses, the water viscosity is unchanged when comparing isothermal (injection water has the same temperature as the reservoir rock) and non-isothermal (injection water has a different temperature than the reservoir rock) injection cases. Two cases are considered: (1) injection water temperature of 400 K (isothermal case) and (2) injection water temperature of 320 K (non-isothermal case). Injection begins at time $t = 0$ and is specified at a constant rate of $0.6 \times 10^{-7} \text{ m}^3/\text{s}$ per meter thickness of reservoir. The problem does not consider the possibility of natural fracture deformation under initial in situ stress and pore pressure fields. Variations of density or viscosity with temperature are neglected during simulations. Further problem specifications are provided in Section 10 of White et al. (2016b).

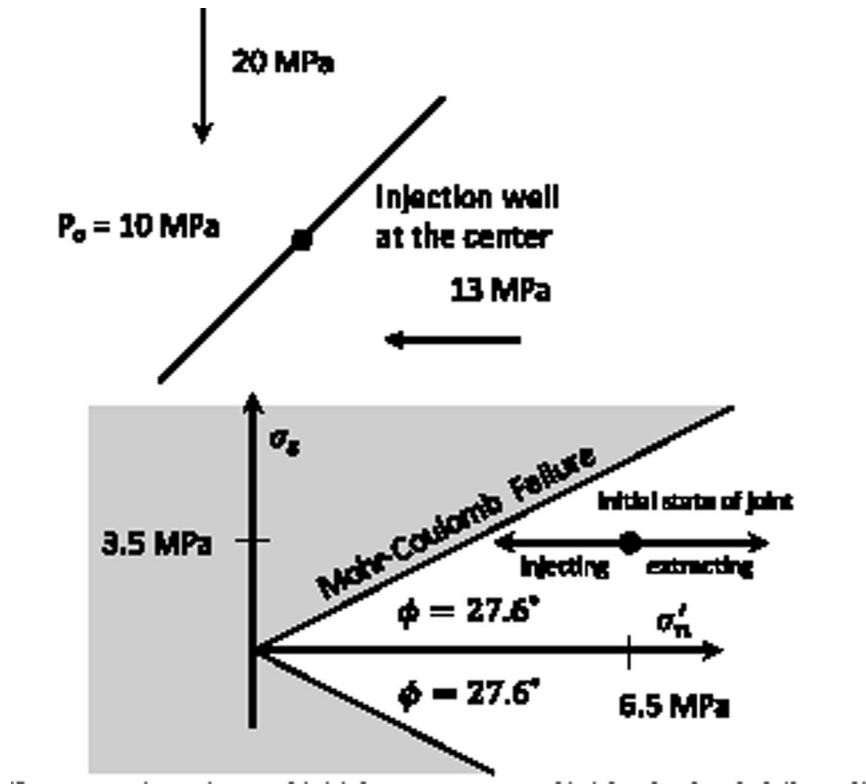
Five teams submitted results for this geochemical problem, as listed in Table 11. Because the physics of the problem was not constrained and some teams included poroelastic stresses in the matrix rock while others did not, the results are presented separately for each set of assumptions. Stanford submitted results for both assumptions and both cases (isothermal and non-isothermal). Figure 15 illustrates the pressure with injection time for the isothermal case where poroelastic stresses are considered. While the curves have

similar shapes, the Stanford model predicts a slightly higher pressure. For the isothermal case in which only pressurization of the fracture was considered, the results for pressure versus time are also in good agreement.

Aperture variation with injection time was simulated for the isothermal case with poroelastic stress, for the isothermal case without poroelastic stress, and for the non-isothermal case with poroelastic stress. Note that cooling tends to increase the fracture aperture, however, in view of the low temperature contrast (ΔT) between the injection water and the rocks and the low value of thermal diffusivity, thermal stress is not very large and develops very slowly. The thermal stress effect is focused in the central region of the fracture where most cooling occurs, and it expands with time. Increasing ΔT increases the cooling-induced crack opening. Note also the contrast between the profiles for the isothermal and cooling cases. It should be emphasized that cooling in the crack is controlled by the residence time of the fluid which is influenced by injection rate and leak-off, and fracture permeability.

The shear deformation along the fracture length 72 days into the simulation and at the end of the simulation (180 days) was additionally computed. Simulation results compare quite favorably for the isothermal case in which poroelastic stresses are considered (Fig. 16). For the isothermal case in which

Fig. 14 Fracture orientation and initial stress state; and Mohr–Coulomb failure diagram



poroelastic stresses are not considered, the OU and Stanford results differ in early time, but converge to nearly the same solution by the end of the simulation. The non-isothermal case also shows the same pattern of timing.

3.7 Benchmark problem 7: surface deformation from a pressurized subsurface fracture

3.7.1 Problem champion: Pengcheng Fu, Lawrence Livermore National Laboratory

This problem is largely based on the work of Pollard and Holzhausen (1979) and entails the calculation of ground surface deformation in response to fluid injection into a subsurface fracture. The fluid pressure is assumed to act uniformly over the fracture surfaces and the fracture is idealized as being rectangular in shape, oriented at various dipping angles. The rock matrix is assumed to have isotropic-homogeneous properties and the mechanical characteristics are to be modeled as being linear elastic. The problem was posed in both 2- and 3-dimensional forms. In

3-dimensional form the fracture is specified as being $2a$ wide and $2b$ long, with the coordinate system centroid being located on the ground surface, vertically (y -direction) directly above the centroid of the fracture. The z -direction coordinate system axis is oriented with the length of the fracture and the x -direction is oriented with dipping or width direction. The dipping angle is respect to a horizontal axis. The in situ stress is assumed to be isotropic and the specified net fluid pressure is difference between the normal in situ stress on the fracture and the actual fluid pressure. A static solution to the problem is sought, ignoring the transients. Metrics for the problem are the vertical surface displacements from $x = -4a$ to $x = 4a$ for dipping angles of 0° , 45° , and 90° . Additional metrics are the mode-I and mode-II stress intensity factors at the two fracture tips.

As illustrated in Fig. 17, the rectangular fracture is $2a$ wide and $2b$ long with a dipping angle β . A global coordinate system and a local coordinate system are created. The origin of the global x – y – z coordinate system is at the projection of the fracture center on the ground surface. The y -axis is along the vertical

Table 11 Participating teams and computer codes for benchmark Problem 6

Simulation team	Code(s)
Pennsylvania State University (PSU)	FLAC ^{3D} and TOUGHREACT
Stanford University (Stanford)	CFRAC
University of Nevada, Reno (UNR)	MULTIFLUX and TOUGH2
The University of Oklahoma (OU)	GEOFRACT
The University of Texas at Austin (UTA)	CFRAC-UT

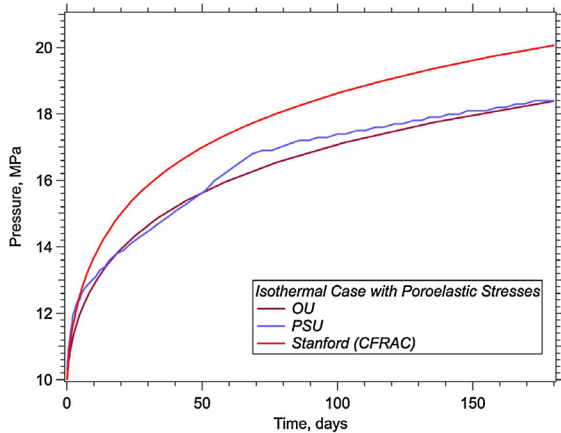


Fig. 15 Simulation results for pressure versus time for the isothermal case in which poroelastic stresses in the matrix rock are considered

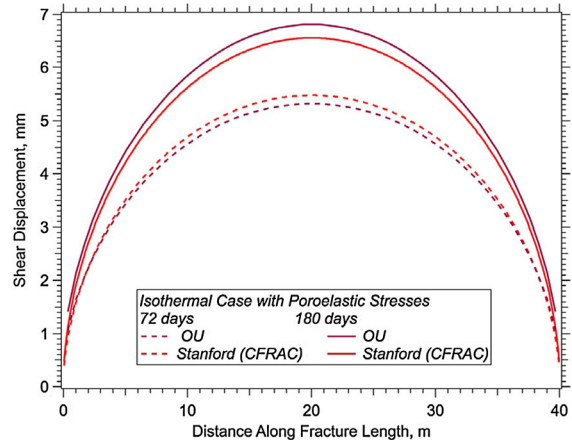


Fig. 16 Simulation results for shear deformation along the fracture length at 72 days and 180 days for the isothermal case in which poroelastic stresses in the matrix rock are considered

direction pointing upwards and the z-axis is along the strike direction. The origin of the local u-v coordinate system is at the fracture center. The u-axis is along the strike or the length direction while the v-axis is along dipping or the width direction. The fracture center is at a depth of d so the u-v coordinate system's origin ($u = 0, v = 0$) has a coordinate $(0, -d, 0)$ in the global coordinate system. If $b \gg a$ and $b \gg d$, this three-dimensional (3D) geometry can be modeled as a two-dimensional (2D) plane-strain problem. The 2D geometry is essentially a vertical cut of the 3D model in the x-y plane. Note that the coordinate system is problem-dependent and each problem in the present paper establishes different coordinate systems.

If *in situ* stress is concerned, the pressure applied on the fracture surfaces (P_0) should be considered the “net pressure”, which is the difference between the fluid pressure and the *in situ* normal stress acting on the fracture plane. Anisotropy of *in situ* stress will not affect the results if the fracture happens to be horizontal or vertical ($\beta = 0^\circ$ or 90°), but will affect the results for oblique fractures (e.g. $\beta = 45^\circ$) due to

the shear stress on fracture faces. Therefore, the setup of the problem implies isotropic *in situ* stress. Further problem specifications are provided in Section 11 of White et al. (2016b). All results are presented in a non-dimensional form, with units only given to add some engineering reference to the problem.

Six teams submitted results for this problem, three teams submitting both 2D and 3D results, two teams submitting only 2D results, and one team submitting only 3D results, as listed in Table 12. Results submitted by the five teams for the 2D problem are shown in Fig. 18 for the dipping angles $\beta = 45^\circ$. The calculated robust averages, robust standard deviations, and ISO 13528 uncertainties are also shown. Overall the results match each other very well. Particularly, the results submitted by INL, Itasca, and LLNL are almost identical to each other and to the results in (Pollard and Holzhausen 1979) for all three dipping angles. The results of OU over-predict the median predicted surface deformation and those of PSU seem to slightly under-predict. The differences are relatively small (within 7%) but the trend of over-/under-prediction is

very consistent among all dipping angles simulated. Because the differences between the OU/PSU results and the rest are not only in the overall vertical locations of the curves, but also in the vertical distances between the highest and lowest points along the curves, they could not have been caused by the difference in domain sizes used by different teams. They likely reflect differences in the formulations and solution methods of the codes or meshing densities and configurations.

Four teams submitted 3D surface deformation results, among which the UTA team only obtained results for $\beta = 90^\circ$ as the new 3D implementation of CFRAC_UT only handles vertical fractures (McClure et al. 2015). The results for the dipping angle $\beta = 90^\circ$ and x-axis sampling line are shown in Fig. 19. As the plane-strain 2D model is equivalent to a 3D model with infinite out-of-plane depth (i.e. b approaches infinity), the 3D surface deformation at $z = 0$ is expected to be smaller than the 2D solution. The 3D solutions overall are very similar to each other, although the difference is somewhat more pronounced than that for the 2D results. For $\beta = 0^\circ$ and 45° , the OU solutions still over-predict the surface deformation, consistent with the trend in 2D. For the case with

$\beta = 0^\circ$, the OU deformation is even greater than the 2D reference solution, a clear evidence of some inaccuracy. However, the OU 3D deformation is smaller than their 2D deformation, passing a self-consistency check. For the case with $\beta = 90^\circ$, the results of all four teams are very similar, showing smaller surface deformation than the 2D reference solution, as expected.

4 Challenge problems

Two challenge problems were developed; both addressing specific questions via numerical simulation in three topical areas: (1) reservoir creation/stimulation, (2) reactive and passive transport, and (3) thermal recovery. Questions were developed for each challenge problem and topical area, and are detailed in the companion problem-statement document (White et al. 2016a). Challenge Problem 1 considers the Phase II Reservoir at Fenton Hill, located at true-vertical depths between 3283 and 3940 m, between wells EE-3A and EE-2A. Challenge Problem 2 considers the shallower Phase I Reservoir at Fenton Hill, located at true-vertical depths between 2615 and 2758 m, between wells EE-1 and GT-2B. Problem champions for Challenge Problem 1 were Derek Elsworth, Departments of Energy and Mineral Engineering and Geosciences, Penn State University, and Eric Sonnenthal, Earth Sciences Division, Lawrence Berkeley National Laboratory, and for Challenge Problem 2 were Pengcheng Fu, Atmospheric, Earth and Energy Division, Lawrence Livermore National Laboratory and George Danko, Mining Engineering Department, University of Nevada, Reno. Full problem descriptions were described by the GTO-CCS Challenge Problem champions (White et al. 2016a). Solutions to the GTO-CCS Challenge Problems in selected topical areas have been previously published (Danko et al. 2016; Fu et al. 2016; Gao and Ghassemi 2016; Mudunuru et al. 2016; Norbeck et al. 2016a). This paper provides a synopsis of the solutions to the GTO-CCS Challenge Problems submitted during the study, both those which have been previously published and those which have yet to be published, and then provides a discussion of the outcomes of the collaborative nature of this code comparison study.

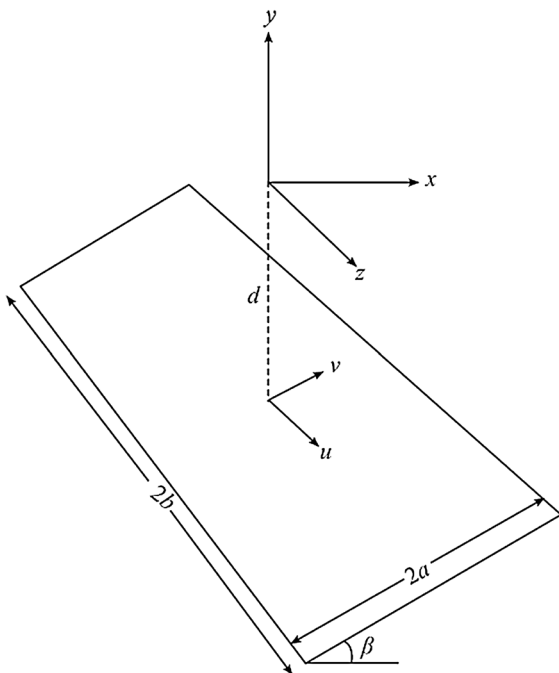


Fig. 17 Geometry of the fracture in three-dimensions and the coordinate systems

Table 12 Participating teams and computer codes for Benchmark Problem 7

Simulation team	Code(s)	Dimensions
Idaho National Laboratory (INL)	FALCON	2D
Itasca Consulting Group (Itasca)	FLAC ^{3D}	2D/3D
Lawrence Livermore National Laboratory	GEOS	2D/3D
Pennsylvania State University (PSU)	FLAC ^{3D} and TOUGHREACT	2D
The University of Oklahoma (OU)	GEOFRAC	2D/3D
The University of Texas at Austin (UTA)	CFRAC-UT	3D

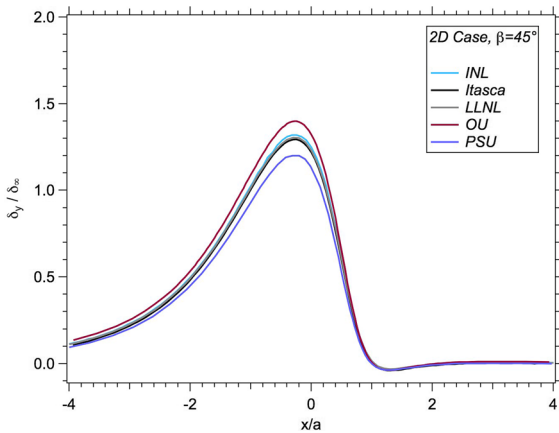


Fig. 18 Vertical surface displacement δ_y normalized by δ_∞ from $x = -4a$ to $4a$ for $\beta = 45^\circ$ for the 2D scenario

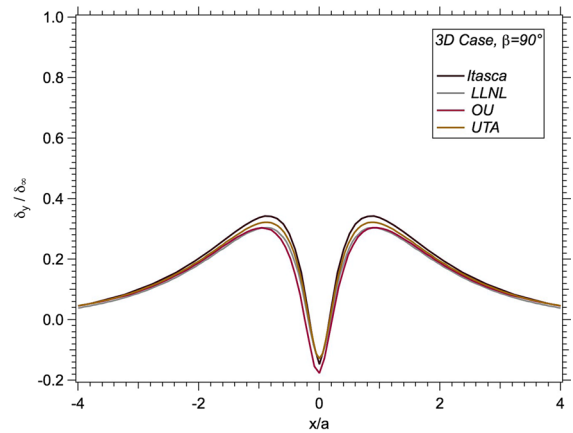


Fig. 19 Vertical surface displacement δ_y normalized by δ_∞ from $x = -4a$ to $4a$ for $\beta = 90^\circ$ for the 3D scenario

4.1 Challenge problem 1: Fenton Hill Phase II reservoir

4.1.1 Problem champions: Derek Elsworth, Pennsylvania State University and Eric Sonnenthal, Lawrence Berkeley National Laboratory

The Phase II Reservoir at the Fenton Hill test site, located near Los Alamos, New Mexico, USA, was designed to test the enhanced geothermal system concept in hot dry rock at temperatures and geothermal heat production rates near those required for a commercial electrical power plant. Phase II field activities at Fenton Hill started with the drilling of well EE-2 on April 3, 1979 and ended with reservoir circulation being discontinued on July 14, 1995, following an annular breakthrough in the injection well EE-3A. The culminating experiment at Fenton Hill was the Long-Term Flow Test (LTFT), which lasted 39 months, with 11 months of active circulation through the reservoir. The Phase II Reservoir at Fenton

Hill comprised a single injection well, EE-3A and a single production well, EE-2A, which were hydraulically connected via a complex joint network in otherwise impermeable hot rock. Tracer tests conducted during the LTFT indicate, via the nature of the tracer recovery profiles during steady-flow operation periods, that reservoir fluid pathways were becoming longer over time; an indication of shorter pathways being closed off. Temperatures across the four fluid-entry points in the open-hole portion of the production well EE-2A during the LFTF show a decline in temperature over time of 7.2 °C at the deepest point and 1.8 °C at the shallowest point. Because continuous long-term circulation periods were not fully achieved within the Phase II Reservoir at Fenton Hill, there remains uncertainty about the thermal recovery performance of the reservoir over an extended period of time.

This problem seeks solutions via numerical simulation that answers specific questions concerning the Phase II Reservoir at Fenton Hill, in three topical areas: (1) reservoir creation/stimulation, (2) reactive

and passive transport, and (3) thermal recovery. The response of the Phase II Reservoir to fluid injection and production is considered to be governed by strongly coupled hydrologic, thermal, geomechanical, and geochemical processes. Solutions shall address the coupled nature of these processes and demonstrate consistency with the experimental observations made during the reservoir creation and circulation tests as part of the Phase II Project at Fenton Hill. Models of the hydraulic connection between wells EE-3A and EE-2A can be conceptual or fracture networks generated via numerical simulation of the Phase II reservoir development via the hydraulic stimulation. Within the descriptions of each of the three topical areas, problem statements will include a question, metrics, and output section. The metrics section includes key experimental observations made during the Phase II Project at Fenton Hill, but the study encouraged solution submissions that utilized additional metrics to demonstrate coupled processes or defend submitted solutions. Problem specifications for Challenge Problem 1 are provided in White et al. (2016a).

4.1.2 University of Nevada, Reno

The team from University of Nevada, Reno (UNR) developed a new fracture and flow system modeling methodology (Danko et al. 2016) and applied this methodology to elements of the reactive-transport and thermal recovery topical areas of Challenge Problem 1. Their approach involved developing a network of elliptical planar fractures that connected injection well EE-3A with the production well EE-2, using the three-point location method of clustering the micro-earthquakes. The resulting network comprised 10 fractures with centroids, orientations, and dimensions (i.e., major and minor radii) with the centroid locations and sizes adjusted to match published connectivity by Smith et al. (1989). The fracture planes were then discretized with structured rectangular meshes, allowing for variable aperture across the fracture extent. Principal assumptions of the analysis were isothermal conditions and constant fracture aperture, with reference fracture aperture and pressure aperture coefficient being principal unknowns, determined by executing the fracture network flow model against two stages of the fluid circulation tests, as reported by Duchane (1996). The dynamic behavior of the fracture network to the production well back pressure was

demonstrated, by fracture apertures of 0.094 and 0.103 mm, respectively for production pressures of 9.7 and 15.2 MPa. One principal outcome from this solution submission was that calibration against the experimental circulation flow tests was possible with a simple aperture fracture network model with just two parameters. The UNR team concluded that incorporation of variable fracture aperture and thermal contraction would allow the fracture flow model to predict thermal drawdown, the core question in the thermal recovery topical area for Challenge Problem 1. Further details on the submission by the UNR team are provided in White et al. (2017).

4.1.3 Pennsylvania State University

The team from Pennsylvania State University (PSU) utilized a new numerical simulator, TF_FLAC^{3D}, for modeling a randomly distributed fractured rock mass via an equivalent continuum approach (Gan and Elsworth 2016). This new modeling approach advances the PSU team's capabilities for EGS reservoirs, building on their previous continuum simulator TFREACT (Taron et al. 2009). The key advancement was the ability to model fracture networks within an EGS reservoir without gridding dependence, with the implementation of constitutive equations for stress-dependent permeability, including normal closure, shear dilation, and out-of-contact fracture walls under tensile loading. The critical elements of this development were the mapping of discrete fractures onto a discretized 3-dimensional rock mass volume, the formulation of an equivalent continuum Young's modulus and Poisson ratio, a permeability tensor, a porosity model, and a model for stress-dependent fracture aperture, and the development of an iterative solution scheme to realize convergence. The PSU team demonstrated this new modeling capability against single- and multi-fracture validation problems, with the single-fracture problem being Benchmark Problem # 6: Injection into a fault/fracture in thermo-poroelastic rock. Whereas the equivalent continuum approach adopted by the PSU team differs from the embedded fracture model approach of the Stanford team in terms of requiring additional spatial discretizations to account for the fractures, both approaches recognize the need for modeling discontinuous fracture networks with variable fracture dimensions and orientations.

The PSU team approach to answering the thermal recovery topical area question of Challenge Problem 1 was two staged. During the first stage, fracture networks of the Phase II reservoir were defined from the seismic events recorded during the injection phase of the massive hydraulic fracturing (MHF) Test (Roff et al. 1996), conducted at Fenton Hill and known as Experiment 2032. Fracture networks were developed from the major fault plane orientations reported by Phillips et al. (1997) (i.e., near vertical at -56° strike and 70° strike), using an assumption of 1 fracture in each direction per cluster of 20 seismic events. This resulted in a network with 190 fractures in each of the two principal directions. Fractures lengths were assumed to be normally distributed with a mean of 50/30 m and standard deviation of 20/10 m. Simulations of the 2½-day MHF Test were then executed with the developed fracture network, using the recently developed TF-FLAC^{3D} simulator. Pressure distributions were generated after 3 days of injection at constant rate of $0.1 \text{ m}^3/\text{s}$, approximating the rate of the MHF Test for two presumed principal horizontal stress realizations, oriented $0^\circ/90^\circ$, of 40/25 MPa and 20/13 MPa. The objectives for this stage of the study was to develop a fracture network and fracture properties that yielded agreement with the pressure response of the MHF Test, given the stress state and fluid injection rate.

During the second stage of the study, the PSU team examined the response of two different closed fracture networks; a sparse long fracture network based on a single fracture in each major fault plane orientation reported by Phillips et al. (1997) (i.e., near vertical at $-56^\circ/70^\circ$) per cluster of 80 seismic events with average lengths of 300/200 m, and a dense short fracture network with a single fracture in each direction of average lengths 70/30 m per cluster of 30 seismic events. Simulations were then executed based on the flow rates of the Initial Closed-Loop Flow Test (ICFT) (Brown et al. 2012), for a period of 10 years using the sparse-long and dense-short fracture networks, and two reservoir thicknesses of 50/200 m. An observation from the Fenton Hill project was that a second production well on the stagnant end of the elongated reservoir would be beneficial in terms of increasing productivity. The PSU team's dual production well configuration followed this recommendation. Simulation results revealed significant differences between the thermal

recovery in terms of power and total energy between the sparse-long and dense-short fracture networks, with the dense-short networks achieving roughly 2.75 times the total recovered energy compared with the sparse-long networks. The case for a 200 m thick reservoir returned $\sim 20\%$ higher production rate and a longer thermal life than the 50 m reservoir (for the same mass flow-rate). Stress changes at the end of the 10-year production period in the three principal directions due to thermal contraction and fluid injection were large, yielding fracture permeability increases and potentially tensile opening of some fractures.

The solution submission from PSU provided a new perspective on the performance potential of the Fenton Hill Phase II reservoir, which predicted that $> 20\text{MW}_{\text{th}}$ and $> 7\text{MW}_{\text{th}}$ systems can be operated for initial periods for the dense-short and sparse-long fracture networks. Long term thermal recovery predictions are in general agreement with simulation predictions of 4 MW_{th} production over a 30-year period, but the PSU simulations show more intensive initial production with moderately sharp thermal drawdown after several years. The thermal drawdown behavior is strongly dependent on reservoir thickness. For the 50-m reservoir, strong thermal drawdown occurs after the 2nd year while for the 200-m reservoir the lifetime is approximately three-times longer. Extrapolating the simulations results to 30 years, shows thermal power production falling below 1 MW_{th} around 15 years for both the dense-short and sparse-long fracture networks for the 50-m reservoir thickness. In terms of the objectives of the GTO-CCS Challenge Problem stage, the PSU team recognized the need for modeling fracture networks of random orientations and dimensions, with fracture permeability being stress dependent, including normal closure, shear dilation, and out-of-contact fracture walls under tensile loading and then advanced their simulation capabilities in response. Further details on the submission by the PSU team are provided in (White et al. 2017).

4.1.4 Los Alamos National Laboratory

The team from Los Alamos National Laboratory (LANL) approached the challenge of predicting the long-term thermal recovery performance of the Fenton Hill Phase II Reservoir from a reduced-order modeling

approach (Mudunuru et al. 2016). The founding concept behind reduced order modeling is to develop functions of a limited parameter set that describe the behavior of a complex system. Generally, the parameter sets and functional forms are chosen, and the function coefficients are determined from numerical simulations executed with conventional coupled-process models on the complex system. For this work the LANL team used the PFLOTRAN (Lichtner et al. 2015) simulator to model fluid flow and heat transport within the Phase II Reservoir. For this analysis, the team elected to not consider geomechanical or geochemical effects on the system. The geologic model of the Phase II Reservoir assumed 1000 m × 1000 m × 1000 m rectangular reservoir, with an embedded 650 m × 650 m × 500 m rectangular fracture zone, and both zones having constant density, specific heat, thermal conductivity, and intrinsic permeability. The conceptual model of the Phase II Reservoir included a vertical injection and production well, intersecting the fracture zone, with constant fluid heat capacity, fluid density and fluid injection temperature. The parameter set for the reduced-order model comprised the fracture-zone permeability, production-well skin factor, injection mass flow rate, and bottom-hole pressure. Three reduced-order models were considered to predict the thermal power output from the Phase II Reservoir over a 120-day time period, within the LTFT experiment at Fenton Hill (Brown et al. 2012), using time and fracture-zone permeability as the parameters. Reduced-order models that included the production-well-skin-factor, injection-mass-flow-rate and bottom-hole-pressure parameters were not developed. Estimates of thermal power production for the Phase II Reservoir from the reduced-order models for time periods up to 20 years beyond the LTFT were reserved for future work. An outcome from this solution submission with respect to the objectives of the GTO-CCS Challenge Problem stage was the adaptation of the reduced-order model approach to EGS. Whereas the submitted solution developed reduced-order models for thermal power production solely based on time and a single reservoir parameter, the implementation of an expanded parameter set, and inclusion of geomechanical and geochemical effects will reveal the true potential of applying reduced-order models to EGS operations.

4.1.5 McClure Geomechanics, LLC and Stanford University

The teams from McClure Geomechanics LLC and Stanford University (McCG-Stanford) collaborated to investigate: (1) the hydromechanical behavior during stimulation and (2) the thermal drawdown during long-term circulation. The analysis is described in detail by Norbeck et al. (2016b) and Norbeck (2016). Modeling was performed using the two-dimensional version of CFRAC (Complex Fracturing ReseArch Code), a discrete fracture network simulator that couple's fluid flow with the stresses induced by fracture deformation and porothermoelastic deformation in the matrix. Detailed descriptions of the numerical formulation for the model used in this study are provided in Norbeck et al. (2016c) and Norbeck and Horne (2016).

The interpretation of the hydromechanical behavior was based on the following observations: (1) injectivity increased very sharply and nonlinearly at a threshold bottom hole pressure (BHP); (2) at BHP less than the threshold pressure, injectivity was low and did not increase significantly from one injection sequence to the next; and (3) the microseismic cloud formed an ellipsoidal region with the long axis nearly north–south (with a slight rotation to the west), very different from the direction of the maximum principal stress (N30°E). The orientation of the stresses is known from the orientation of breakouts in acoustic borehole televiewer logs. According to conventional geomechanical theory (Zoback 2007), observation (1) suggests that hydraulic fractures formed and propagated through the formation. Observation (2) suggests that shear stimulation caused minor or negligible increase in injectivity. Observation (3) is seemingly contradictory with observation (1) because in the far-field, hydraulic fractures form perpendicular to the minimum principal stress. The long axis of the ellipse should form in the direction perpendicular to the minimum principal stress; the shorter axis of the microseismic cloud forms as fluid leaks off from the hydraulic fracture into the surrounding formation, triggering microseismicity.

The McCG-Stanford team focused on reconciling the contradiction between observations (1) and (3). Three hypotheses were considered: (a) the orientation of the maximum principal stress was not actually N30°E; hydraulic fractures formed at the well and

propagated perpendicular to the (true) minimum principal stress; the long axis of the microseismic cloud is, in fact, in the direction of maximum horizontal stress; (b) at the well, hydraulic fractures formed at the well and propagated through the formation perpendicular to the minimum principal stress; away from the well, they intersected large, permeable fault zones; subsequently, fluid flow occurred dominantly down the faults, causing the microseismic cloud to orient in the direction of the strike of the large faults; (c) stimulation occurred through the 'mixed mechanism' conceptual model described by McClure and Horne (2013, 2014); hydraulic fractures were unable to form at the wells because of the high tensile strength of the granitic rock; the threshold BHP corresponded to the normal stress on the natural fractures in the formation that intersect the well, which were jacked open; hydraulic fractures were able to form as splays off the natural fractures or from extension from the tip; the hydraulic fractures terminated against natural fractures due to mechanical interaction; the overall result was a mesh of hydraulic fractures perpendicular to the minimum principal stress and natural fractures oriented at (roughly) N23°W, which led to an overall north–south orientation of the stimulated region.

Hypothesis (a) cannot be entirely ruled out. However, the orientation of the horizontal stresses is known from interpretation of wellbore image logs, which is a highly reliable technique for estimating stress orientation. The orientation could only be incorrect if there was an error during the acquisition of the image log data. Hypothesis (b) seems unlikely because there is no evidence of large, highly permeable faults in the Fenton Hill reservoir. The injectivity of all wells was low, indicating that none intersected a highly permeable fault. Large faults form thick damage zone with characteristic formation of cataclasite and other features, none of which were reported from any core or cuttings collected at the site. Large-scale permeable faults cause convective temperature gradients (low thermal gradient); high thermal gradients were observed at depths at Fenton Hill. The microseismic cloud extended about the same distance from the injection well in both directions, and so hypothesis (b) requires that there were at least two parallel large-scale faults present in the formation, with the injection well coincidentally located midway between them.

Hypothesis (c) is similar to the theory proposed by Brown (1989) and Brown et al. (2012), where the reservoir consisted of two sets of joints—one perpendicular to the minimum principal stress (storing the majority of the injected fluid) and another joint set at a different orientation, bearing significantly higher normal stress. Hypothesis (c) modifies this theory by asserting that the fractures perpendicular to the minimum principal stress were not natural fractures, but instead were generated during the injection and propagated from the mechanically opened natural fractures. Termination of hydraulic fractures against natural fractures is a necessary feature of the hypothesis because otherwise, the hydraulic fractures, once formed, would propagate perpendicular to the minimum principal stress and cause the overall microseismic cloud to orient in their direction of propagation. At the time of the Fenton Hill project, the concept that hydraulic fractures may terminate against natural fractures was not widely recognized in the literature; therefore, it is unsurprising that this mechanism was not considered by Brown (1989). But today, fracture termination against preexisting features is widely recognized as a potentially significant process and is an area of active research, summarized by McClure and Horne (2014). Hypothesis (c) deviates from conventional geomechanics theory (Zoback 2007) in asserting that fluid pressure exceeded the minimum principal stress at the well and did not induce hydraulic fracture propagation directly from the well. However, Section 4.8 from Norbeck (2016) lists several field examples of high rate injection into granite where this has occurred. It is hypothesized that in very high strength rocks such as granite, tensile strength for fracture initiation becomes non-negligible.

Hypothesis (c) implies the minimum principal stress is much lower than implied by Hypotheses (a) and (b). In fact, a discrepancy was noted in the data at the site. Shallower measurements indicated a low stress gradient, while deeper measurements seemed to indicate a much higher stress gradient. Kelkar et al. (1986) interpreted these measurements as indicating a large discontinuity in the stress state at around 3 km depth. Brown (1989) proposed that the lower stress profiled prevailed throughout and that there was a discontinuity in the natural joint orientation at 3 km depth. A mix of strike-slip (SS) and normal faulting (NF) focal mechanisms of the seismic events indicated a transitional SS-NF stress regime with $\sigma_v \cong \sigma_H > \sigma_h$,

where σ_v is the vertical stress, σ_H is the maximum horizontal stress, and σ_h is the minimum horizontal stress. The low-stress-gradient model is what one would expect, given constraints on stress magnitudes, following the assumption of a critically-stressed crust (Zoback 2007). Conversely, the high-stress-gradient model would require a pure SS stress regime (i.e., $\sigma_H > \sigma_v > \sigma_h$) to be consistent with the critically stressed crust assumption at the 3.6 km depth.

Using Hypothesis (c) and the lower stress profile proposed by Brown (1989), the entire injection, shut-in, and flowback history into the Phase II wells (during the stimulation phase) was simulated with CFRAC in a reservoir-scale discrete fracture network in a single continuous simulation (spanning nearly 2 years). The simulations involved propagation of hydraulic fractures as splays off natural fractures, and the propagating fractures subsequently terminated against other natural fractures. The simulation results were consistent with the overall observations—orientation of microseismic cloud and a threshold pressure for mechanical opening of natural fractures (Norbeck et al. 2016b). In order to match the observation that injectivity below the threshold pressure did not increase significantly between injections, it was necessary to specify in the simulation settings that shear stimulation had minor or zero effect. The simulations reproduced the occurrence of the Kaiser effect in subsequent injections and the rate of spreading of microseismicity from the wellbore. Simulations with and without poroelastic and thermoelastic effects were performed.

Next, the simulations were extended to include the several circulation tests that were performed in the reservoir. The simulations were consistent with the spatial and temporal distribution of seismicity that occurred during circulation and consistent with the observation that seismicity only occurred when injection pressure was increased. The simulations were also consistent with the data in showing a drop in reservoir impedance when backpressure was increased at the production well and that there was a decline in water loss to the formation over time. One area of mismatch was that the simulations required bottomhole pressure to be near the in situ reservoir pressure in order to match the observed production rate. In the real data, significant production rates were accomplished with bottomhole pressure much greater than the in situ reservoir pressure. This remarkable observation can

only be explained by positing that there was a strong hydraulic connection between the production and the injection wells. In the simulation, the connection between the wells was affected by the randomness of the discrete fracture network; in the particular simulation run for the study, there as not (by chance) a strong connection. In the Fenton Hill project, the wells were sidetracked and redrilled several times until a good connection was achieved, indicating that the connection observed in the actual data was dependent on fortunate alignment of the wells along a high conductivity fracture.

The conventional theory of EGS stimulation is that injection induces significant shear stimulation. While there is uncertainty between hypotheses (a), (b), and (c), the McCG-Stanford concludes that the data do not support the hypothesis that shear stimulation was the dominant factor in the hydromechanical response of the wells during the injections studied in Challenge Problem 1.

4.2 Challenge problem 2: Fenton Hill phase I reservoir

4.2.1 Problem champions: Pengcheng Fu, Lawrence Livermore National Laboratory and George Danko, University of Nevada, Reno

The Phase I Reservoir at the Fenton Hill test site, located near Los Alamos, New Mexico, USA, was designed to demonstrate the technical feasibility of the enhanced geothermal system concept in hot dry rock. Phase I field activities at Fenton Hill started with the drilling of the GT-2 borehole on February 17, 1974, and ended with the shutdown of final circulation on December 16, 1980. Various tests, including injection and flow-back experiments, well logging and coring, chemical tracer and chemical leaching were performed concurrently with the drilling program. After the establishments of hydraulic connections between the two wells, a series of five circulation tests, referred to as Run Segments 1–5, were conducted in the Phase I Reservoir. Heat was produced from two different stimulated fractures/fracture networks in Run Segments 1–3 and in 4–5. A full set of evidences suggest that the sub-reservoir producing heat in Run Segments 1–3 consists of a major fracture intersecting Well EE-1 at 9050-ft (2758-m) depth and Well GT-1B at 8769-ft (2673-m) depth. The majority of the circulated fluid

entered into the major fracture via the intersection with Well EE-1 and exited from the fracture through the intersection with Well GT-2B. Temperature logs along the wellbore indicated that the flow entry points at 8620 ft (2627 m) and 8900 ft (2713 m) in Well GT-2B also contributed to the flow. The hydraulic impedance of the producing reservoir was very low, especially when a high backpressure was applied to dilate the fracture. The fracture that produced heat during Run Segments 1–3 was of modest size and substantial thermal drawdown had taken place. The sub-reservoir responsible for Run Segments 4 and 5 was of a much larger volume and only limited thermal drawdown evolved during the 9-month Run Segment 5 circulation. However, the high hydraulic impedance and its insensitivity to backpressure suggested that the reservoir was likely composed of multiple intersecting fractures under high confining stresses. However, the available evidence was insufficient to constrain a definite fracture network model. Challenge Problem 2 seeks solutions via numerical simulation that answer specific questions concerning the Phase I Reservoir at Fenton Hill, in three topical areas: (1) reservoir creation/stimulation, (2) reactive and passive transport, and (3) thermal recovery. Problem specifications for Challenge Problem 1 are provided in (White et al. 2016a).

At this writing four teams have submitted solutions against the Reservoir Creation and Stimulation topical area of Challenge Problem 2 while no systematic analysis of the other two components of the problem was presented, likely due to the limited time and resources that the teams had. The Reservoir Creation and Stimulation component concerns a series of five pressurization and venting experiments in Zone 7 of well GT-2 after stage 2 drilling of Fenton Hill Phase I, performed in September 1974. These experiments provided intriguing field observations that make it possible to infer the hydraulic stimulation mechanism involved. Zone 7 is the open-hole interval at the bottom of well GT-2 after stage 2 drilling (2043 m deep). Field observations indicated that two natural joints between 1990–1993 and 1999–2000 m deep, respectively, approximately dipping 70°, might have been opened by the stimulation. Key observations from the five injection, shut-in and subsequent venting experiments included the following: (1) pressure limiting behavior—injectivity rapidly increased once the wellhead pressure reached 17.2 MPa (2500 psi);

(2) shut-in pressure declined after the first injection exercises, as depicted in Figs. 3, 4, 5, 6, 7, 8 and 9 of Brown et al. (2012); (3) there was small flow-back ratio of the injected water after the first four water injection experiments; and (4) there was very high fluid recovery ratio after the fifth injection, which used cross-linked gel mixed with sand. Each participating team was asked to simulate these injection, shut-in, and flow back operations, using assumptions consistent with conditions reported in Brown et al. (2012) and other Fenton Hill related publication, with the objective of reproducing these field observations and offering insight into the associated stimulation mechanisms.

4.2.2 Problem refinement via group discussions

The definition of the problem was refined, mostly in the form of clarifications on field observations and physics that needed to be incorporated, based on discussions among the teams tackling this problem, consulting with key participants in the original Fenton Hill study, and preliminary simulations by the problem champion and interested teams. A complication in the interpretation of the fifth test (gel injection with proppant), discovered by Mark McClure, was that a simple volumetric analysis generated some uncertainty about whether proppant actually entered the formation. Based on the well completion dimensions of well GT-2, as shown in Figs. 3, 4, 5, 6, 7 and 8 (Brown et al. 2012), the wellbore volume was around 21–25 m³. However, during the proppant injection period, only 17 m³ of fluid were injected. This simple volumetric analysis suggested that gel-proppant mix could not have displaced all the fluid in the wellbore allowing it to enter the formation/fracture.

Don Brown (personal communication with Mark McClure) indicated that there was field evidence to support proppant having entered the formation because the injection pressure sharply increased by several 10 s of psi a few minutes before shut-in. An interim solution that allowed the participants to proceed with their model building while the problem was further investigated was to assume that because the proppant is denser than water, it settled downward through the well faster than the fluid being pumped. An explanation that McClure worked out and most participants found to be convincing was that the more viscous gel tends to only displace the less viscous

water near the center of the wellbore due to mechanisms presented in Tehrani (1996). Therefore, the gel only needed to displace a fraction of the water in the wellbore to enter the formation, so the interim assumption was appropriate and did not have a negative impact on the resultant simulations.

Some participants raised questions regarding the potential role thermal stress could have played in the five injections tests. The problem champion simulated heat exchange between the injection fluid and the wellbore, cooling of the rock surrounding the fracture, and thermal stress caused by the cooling using a THM coupled model based on LLNL's GEOS code. The results show that great tensile stress (up to 50 MPa tensile stress increment) could develop due to the cooling; this stress component is parallel to the fracture plane and is constrained within a small distance from the fracture. This could have resulted in many short, parallel fractures perpendicular to the fracture plane but such thermal fracturing does not contribute to the four phenomena that we tried to investigate. The thermal stress perpendicular to the fracture plane is approximately 1.3 MPa, a small fraction of the in situ stress.

4.2.3 McClure Geomechanics LLC

McClure Geomechanics LLC (McCG) simulated Challenge Problem 2 with the 3D version of CFRAC, which includes proppant transport and fracture closure onto the proppant placed in the fracture (Shiozawa and McClure 2016). The results were summarized by Fu et al. (2016). The entire sequence of five injections over several days (with either flowback or shut-in between the injections) was modeled in a single continuous simulation. All five injections showed a consistent threshold bottomhole pressure at which injectivity transitioned from being very low to very high. This is interpreted as indicating mechanical opening of a fracture—either a natural fracture or a newly forming hydraulic fracture. In the simulations, it was assumed that there was a single preexisting fracture normal to the minimum principal stress. For the purposes of matching the data in Challenge Problem 2, the exact orientation of the natural fracture and the stress state is non-unique—all that matters is that the normal stress on the fracture is consistent with the observed threshold pressure for jacking. The model assumed that injection occurred at a specific

depth point on the well—as if a fracture was intersecting the vertical well obliquely. If the model had assumed an axial vertical hydraulic fracture formed, this may have had some effect on the results.

If the fracture were not perpendicular to the minimum principal stress, then it would slide in response to injection. However, the data indicated that there was low injectivity prior to reaching the threshold BHP in all five injections. This implies that shear stimulation was minor or negligible and that mechanical opening dominated the hydromechanical behavior (whether or not significant fracture shear occurred). This interpretation is consistent with the interpretation presented in Sect. 4.1.4 for the Phase II reservoir. It should be noted that shear stimulation has been widely accepted in the EGS community as being the primary control on hydromechanical behavior during stimulation, yet in both Challenge-Problem datasets, McCG and Stanford interpret that fracture mechanical opening is the dominant process, compared to shear stimulation. These observations are consistent with the theory of McClure and Horne (2014), who proposed that shear stimulation is the dominant mechanism only in formations with large, preexisting, high permeability faults (which arguably constitute the minority of historical EGS projects).

Simulation parameters were varied to match the pressure transient trend during shut-in after the initial injection period. The transient was controlled by two parameters affecting the magnitude and effective stress sensitivity of the aperture when the fracture is mechanically closed. These parameters were varied until a very close match to the transient was achieved. Because of the uncertainty about whether proppant entered the formation during the final injection period, two simulations were performed. In the first, it was assumed that no proppant entered the formation. In the second, the full proppant transport and fracture closure algorithm developed by Shiozawa and McClure (2016) was implemented to capture the placement of proppant during the final injection.

The simulation without proppant indicated a much higher fluid recovery after the fifth injection than after the previous injections. Significantly, this occurred without either shear stimulation or proppant entering the formation. Prior to the fifth injection, each injection was performed with greater volume and duration than the previous, causing stimulation to extend further and further from the well and allowing

more time for leakoff (both factors reduced fluid recovery). A large volume of fluid leaked off from the fracture during the previous injections, pressurizing the surrounding matrix and reducing leakoff rate in subsequent injections. The fifth injection used a much smaller volume of fluid and shorter injection duration than the previous injections. These factors, and the pressurization of the surrounding matrix during the previous injections, resulted in much higher fluid recovery after the fifth injection.

In the simulation with proppant, the proppant was placed into a roughly radial region around the injection point. After closure, the proppant greatly increased fracture conductivity and significantly increased fluid recovery. McCG concludes that the greater fluid recovery in the fifth injection is due to the smaller injection volume, the pressurization of the surrounding matrix during the previous injections, and probably (though not necessarily) proppant entering the formation.

The interpretation from McCG differs from some other groups in finding that the observations cannot be explained by the hypothesis that there was shear stimulation or any other irreversible change in the hydromechanical properties of the fracture as a consequence of injection. It is not known whether or not injection induced slip (this depends on the unknown orientation of the fracture inferred to be intersecting the well). If injection did induce slip, then (because of the Kaiser effect) the slip would have occurred during the earlier injection periods and not during the (lower volume) final injection. The same argument applies to any other irreversible process for changing the fracture conductivity; if fracture conductivity changed irreversibly in response to injection, this would have already occurred during the first four injections. Yet fluid recovery was high only after the final injection. There is laboratory evidence to suggest that cycling of open/closing causes hysteretic change in fracture conductivity, but the evidence indicates that cycling causes conductivity to decrease, not increase, due to wear of asperities (Barton et al. 1985). If anything, this effect would have decreased, not increased, fluid recovery in the final injection.

It cannot be ruled out that there were irreversible changes in fracture properties, but these processes cannot explain why recovery was much higher in the final injection. If they occurred, the data suggests that they were secondary effects relative to the dominant

effect of mechanical opening of the fracture when pressure reached its normal stress. McClure and Horne (2014) discussed the experiment in Challenge Problem 2 and hypothesized that the fluid recovery was affected by propagation of splay fractures from an obliquely oriented natural fracture that was opened at the wellbore (similar to the conceptual model used in Sect. 2.4 of this manuscript). While the findings in this section do not rule out this mechanism, they indicate that it is not necessary to explain the observations; more parsimonious explanations are possible.

4.2.4 Lawrence Livermore National Laboratory

Although LLNL's model was also based on an explicit representation of the fracture(s), similar to McClure Geomechanics LLC's approach, GEOS and CFRAC are based on very different numerical methods: finite-element method + finite-volume method (FEM + FVM) vs. boundary-element method + finite-volume method (BEM-FVM). LLNL's modeling assumed that a large vertical fracture plane, 800 m × 800 m in size, centered at the wellbore intersection is embedded in the impermeable rock body. The fluid viscosity was assumed to be 1 cP for the first four tests, and 10 cP for Test 5. Proppant transport was not explicitly simulated; instead, we assumed a "propped" zone, 20 m in radius around the injection point, loosely based on the proppant simulation results of the McClure team. The fracture aperture in this zone was assumed to be not smaller than 30% of the maximum aperture experienced by the corresponding area during the fluid injection. At the commencement of a venting stage following injection, a pressure boundary condition was applied at the intersection between the fracture and the wellbore, forcing the fluid pressure to linearly decrease from the shut-in pressure to the hydrostatic pressure in 5 min and remain at hydrostatic thereafter.

LLNL's simulations of Tests 1 through 4 showed a strong tendency of the injected fluid to migrate upwards once it enters the fracture from the wellbore. This is mainly due to the fact that the vertical gradient of the closure stress on the fracture is much greater than the hydrostatic gradient. Consequently, the fluid continued to move upwards along the fracture during venting instead of flowing downwards to the wellbore. Additionally, the near-wellbore aperture during venting is very small due to the low effective stress near the

wellbore during venting (i.e. the near-wellbore region of the fracture is choked), which also prevented fast flow-back. In the simulation of Test 5 where gel and proppants were used, high fluid viscosity remarkably impedes the upward tendency of the fluid migration. The aperture near the wellbore was dilated to at least 3 mm during injection. Such a large aperture allowed the proppant to enter the fracture, which in turn retained a relatively large aperture during venting. The combined effect of these two factors, namely fluid staying near the wellbore and smaller near-wellbore impedance, results in very high (considerably higher than the injection rate) flow-back rate in the beginning of the venting. The simulation results show that less than 3% of the fluid flowed back in each of the first four tests whereas more than 80% of the injected fluid flowed back in Test 5. LLNL's simulations are highly consistent with the field observations and offer insight into simple yet definitive mechanisms behind the observations.

A detailed comparison between McClure Geomechanics LLC's model and LLNL's model in terms of simulation approach and results has been presented in Fu et al. (2016). Despite their similarity in that fluid was injected into a pre-existing natural fracture, the two teams' models are substantially different from each other in a number of aspect such as numerical approaches, assumptions on fluid viscosity, and assumed dimensions of the fractures. However, both sets of models capture the most important field observations, including the shut-in pressure behavior and the fluid recovery ratios for different injection scenarios quite well. This modeling exercise proves a natural fracture(s) having been opened during the stimulation is a plausible hypothesis.

4.2.5 The University of Oklahoma

The team from The University of Oklahoma (OU) applied numerical simulators, developed by the faculty and students from the OU Mewbourne School of Petroleum and Geological Engineering for addressing problems involving coupled thermal–hydrological–mechanical processes for three-dimensional geologic domains, such as nuclear waste repositories, petroleum reservoirs, and enhanced geothermal systems, in an innovative fashion to the Phase I Reservoir at Fenton Hill. The OU developed simulators solve fully coupled equations for three-dimensional

geomechanics, heat transport, and saturated fluid flow using finite-element spatial discretization with hexahedral shaped elements, having eight nodes per element. This formulation results in five unknowns per node; displacements in the three principal directions, pore fluid pressure, and temperature. For the Fenton Hill application fractures were assumed to be pre-existing and were explicitly modeled as elements within the finite-element grid, with the element having a width much larger than the fracture aperture. The OU team verified this numerical simulator against the Terzaghi one-dimensional consolidation problem, for which there is an analytical solution (Francesco 2013). Agreement was additionally shown for a nonisothermal consolidation against solutions published by Noorishad et al. (1984). A key element of the OU numerical simulator is the continuum damage approach (Lee and Ghassemi 2009) taken to model the joint reactivation or failure process.

The OU team chose to address experiments conducted during late September 1974 within the Phase I reservoir at Fenton Hill, involving a series of 5 reservoir stimulation injections of water into the open borehole section of well GT-2 between depths of 1981–2043 m (6498–6702 ft), known as Zone 7. The first injection being one of short duration (i.e., 1 min) and the final injection including a cross-linked polymer and sand proppant. Joint parameters and grid sensitivity were determined from comparison simulations completed against the first stimulation test, including a zero-stress aperture of 100 μm , a joint stiffness parameter (α) of 200, effective normal stress at an $[\alpha/(\alpha + 1)]$ reduction in aperture of 10 MPa, and a residual aperture of 0.1 μm . For grid sensitivity, 10- and 5-m sized fracture elements were considered. With these parameters, good agreement between the joint opening pressure and the pressure decay profile were noted for a minimum horizontal stress of 34 MPa. The four remaining injection experiments were modeled via three approaches: (1) constant joint stiffness parameter (α) (2) a decaying joint stiffness parameter (α) and (3) a linear relationship between joint stiffness (α) size of the reactivated joint.

The stages of the OU submissions against the GTO-CCS Challenge Problem 2 represented the benefit of the collaborative approach to the code comparison study, as the team re-evaluated their modeling approach with each GTO-CCS presentation, ultimately resulting in a mechanistic model. An

unresolved aspect of the injection experiments conducted in September 1974 in the GT-2 well, was the reason for the near 98% recovery of the water injected during the final injection, versus recoveries of less than 50% for the three previous injections. Brown et al. (2012) attributed this to the inclusion of a sand proppant in the final injection. The OU team opted to find an alternative explanation, given a recent evaluation during the GTO CCS that the volume of proppant-laden fluid was not sufficient to fill the well bore. In their first submission, the OU team was unable to match the final injection recovery without manually altering the residual aperture, for a fixed joint stiffness. In the second submission, the OU team noted good agreement with the experimentally observed fluid recoveries, when the joint stiffness was reduced with each injection. In the third submission, reported at the 50th U.S. Rock Mechanics/Geomechanics Symposium (Gao and Ghassemi 2016) the team successfully demonstrated a new relationship between joint stiffness and the size of the reactivated joint that agreed with the Phase I Reservoir stimulation experiments. In terms of the objectives of the GTO-CCS, the outcomes from the OU team, offered numerical simulations that supported the theory that the fracture network comprised pre-existing natural fractures that were initially sealed and no hydraulic fracturing occurred, but challenged the notion that sand proppant was solely responsible for the high fluid recovery noted in the final stimulation test.

4.2.6 Lawrence Berkeley National Laboratory

The team from Lawrence Berkeley National Laboratory (LBNL) had well established and internationally recognized capabilities for modeling coupled THM processes via their coupling of the TOUGH and FLAC^{3D} simulators (Rutqvist 2017; Rutqvist et al. 2002), and chose to put those capabilities to bear against the reservoir creation and stimulation topical area of Challenge Problem 2, concerned with the Phase I Reservoir at Fenton Hill. This challenge problem addresses the series of experiments conducted during late September 1974 involving a suite of 5 reservoir stimulation injections of water into the open borehole section of well GT-2 between depths of 1981–2043 m (6498–6702 ft), known as Zone 7. The LBNL team modeled this system as a well intersecting a finite thickness fracture element, tilted 70°, within a

finite volume computational domain. This modeling approach was adopted from a previous investigation of fault activation in shale (Rutqvist et al. 2015). Key elements of the approach were an exponential expression for fracture aperture versus effective normal stress, an anisotropic plasticity model allowing shear and tensile failure, strain-softening plasticity to represent sudden slip, and seismic moment and magnitudes from the Kanamori model (Izutani and Kanamori 2001). Prior to modeling the series of injection experiments the LBNL team considered the potential for shear activation of a fracture oriented with a 70° tilt at the known depths for fracture intersections with well GT-2 within zone 7, with vertical stress of 53 MPa, minimum horizontal stress of 34 MPa, initial pore fluid pressure of 20 MPa, fracture cohesion of 1 MPa, and friction coefficient of 0.6. This analysis indicated shear slip of the fracture would occur at pore fluid pressures of 27.7 MPa, below the fracture normal stress of 36.2 MPa.

The LBNL modeling approach included the 2 km well length from the ground surface, specifying the experimental processes of injection, shut-in, and venting at the ground surface, as with the field experiment. All 5 injection stages were modeled via a single simulation execution, with the first short injection period being used, as with the approach of the OU team, to calibrate some fracture and well parameters, such as those used to describe the basic stress versus aperture function. Simulations were executed with both 5- and 60-min shut-in periods, and recovery rates were tracked during the shut-in and venting stages. Proppant and high-viscosity fluid effects were not considered in the simulations of the 5th injection period. Simulation results showed pressure fluctuations during the peak pressures due to rupture propagation with fracture shear dilation, and micro-seismic events were predicted with magnitudes between -2 and 0 , due to slip on new fracture patches. A cumulative shear slip of roughly 5 cm was predicted and non-reversible permeability increases occurred with each injection period associated with shear slip, and reversible permeability increases occurred due to non-linear elastic response to pore fluid pressure fluctuations. The simulations showed good agreement with peak field pressure observations, but predicted lower flow recoveries. With respect to the objectives of the GTO-CCS, the LBNL team advanced their EGS modeling capabilities with the

inclusion of algorithms for computing the effect on permeability of fracture opening by changes in effective normal stress and by shear dilation upon shear failure. Moreover, the team demonstrated the potential for progressive fracture aperture opening with each successive injection stage, due to shear dilation.

5 Conclusions

Numerical simulation provides scientists and engineers with analytical tools for understanding complex physical processes and the capabilities of current multiprocessor workstation computers allow the consideration of coupled processes. For EGS, hydrologic, thermal, geomechanical and geochemical processes all contribute to realizing the energy potentials from geothermal resources. The inherent heterogeneity of the earth's crust contributes greatly to the uncertainty in modeling EGS via numerical simulation, but the modeling of more idealized systems provides opportunities for an in-depth understanding of the impacts of design and field operational choices. In 1980 the geothermal community dedicated the annual Geothermal Reservoir Engineering workshop to defining an appropriate role for numerical simulation in terms of investment decisions related to geothermal performance predictions and to assessing the state of development of geothermal reservoir numerical simulators. The technical foundation for achieving the workshop objectives was a code comparison study, which involved six geothermal problems. Whereas the suite of problems considered a variety of geometric configurations and petrophysical property distributions, the principal processes of concern were single-phase flow, two-phase flow, single-phase to two-phase flash, and heat transfer (i.e., TH processes). The benchmark problem study is similar to the 1980 code comparison study in that the objectives are nearly unchanged: an assessment of computer codes for predicting the power potential and longevity of geothermal reservoirs. Today's numerical simulators for EGS, however, have evolved from those of the 1980s, particularly with respect to modeling fracture-dominated processes and coupled processes. In alignment with this transition in simulation capabilities, all of the benchmark problems in this study concerned fractures, either using an equivalent porous medium

representation or a discrete fracture representation, and included coupled process elements of either HM, THM, or THC. This study has demonstrated that while the U.S. EGS simulation community has a diverse set of computational tools with respect to conceptual approaches, they are able to simulate coupled subsurface processes with comparable results, as evidenced by the benchmark problem solutions. The evolution of numerical simulators over the last 35 years has been impressive, but work remains to be done. The collaborative nature of this study has formed the foundation for the EGS simulation community to collectively address field-scale systems, where coupled process modeling will be essential for understanding the system and experimental observations. Confidence in numerical simulation grows from agreement among field experts, especially when diverse perspectives are represented. This study yielded convergence in understanding over the course of each problem via open dialogue and discussions among the participants.

The pioneering work of the scientists and engineers on the Fenton Hill Hot Dry Rock (HDR) Project, from the early 1970s through the mid 1990s, remains relevant in our quest today to understand the creation and sustained thermal production of EGS reservoirs. Modern numerical simulators are analytical tools that provide us with capabilities for predicting both EGS reservoir creation and thermal performance, but more importantly insight into the fundamental hydrological, thermal, geomechanical, and geochemical processes within EGS reservoirs. The Fenton Hill Phase I and II reservoir experiments yielded an extensive amount of experimental data and observations, but also some lingering questions, as masterfully documented in Brown et al. (2012). Challenge Problems of the Geothermal Technologies Office Code Comparison Study (GTO-CCS) were specifically designed to investigate what new insights could be gained by recognized EGS modeling practitioners applying modern numerical simulators to selected questions concerning the creation, flow and transport behavior, and thermal recovery of two separate confined reservoirs at Fenton Hill. Each of the GTO-CCS Challenge Problems were based on one of the two Fenton Hill reservoirs, and were divided into three topical areas: (1) reservoir creation/stimulation, (2) reactive and passive transport, and (3) thermal recovery. For both reservoirs uncertainty remained about the structure of

the stimulated volume and whether it comprises natural fractures, hydraulic fractures, or a combination of fracture types. In terms of reactive and passive transport and thermal recovery the debate over whether the reservoirs would expand, becoming more diffusive or collapse into a few high permeability channels remains open due to the limited lengths of the flow tests in both reservoirs at Fenton Hill.

More than 20 years after the conclusion of the Fenton Hill experiments, scientists and engineers continue to be challenged with developing commercially viable enhanced geothermal systems. The United States Department of Energy, Geothermal Technologies Office (GTO) is funding a collaborative investigation of enhanced geothermal systems (EGS) processes at the meso-scale. This study, referred to as the EGS Collab project, is a unique opportunity for scientists and engineers to investigate the creation of fracture networks and circulation of fluids across those networks under in situ stress conditions. Principal objectives of the project are to develop a number of intermediate-scale field sites and to conduct well-controlled in situ experiments focused on rock fracture behavior and permeability enhancement. Data generated during these experiments will be compared against predictions of a suite of computer codes specifically designed to solve problems involving coupled thermal, hydrological, geomechanical, and geochemical processes. Comparisons between experimental and numerical simulation results will provide code developers with direction for improvements and verification of process models, build confidence in the suite of available numerical tools, and ultimately identify critical future development needs for the geothermal modeling community. Moreover, conducting thorough comparisons of models, modelling approaches, measurement approaches and measured data, via the EGS Collab project, will serve to identify techniques that are most likely to succeed at the Frontier Observatory for Research in Geothermal Energy (FORGE), the GTO's flagship EGS research effort.

The approach and principal objective of the Challenge Problem portion of the GTO Code Comparison Study was to apply established numerical simulators for EGS to the Fenton Hill reservoir problems, collaboratively discuss simulation results, and test new concepts to account for differences between the numerical results and experimental observations.

Unresolved issues would then be used to establish research directions for GTO in the near future, particularly in the interim period between the conclusion of the study and the opening of the Frontier Observatory for Research in Geothermal Energy (FORGE) subsurface laboratory. In this respect, the Challenge Problem portion of the GTO-CCS has largely succeeded, with each of the teams submitting solutions against the Fenton Hill Phase I and II reservoir questions, developing and adapting new modeling approaches in their numerical simulators, and challenging the accepted understanding of the mechanisms by which EGS reservoirs develop. A somewhat unexpected outcome of this study was that the highly collaborative nature of the discussions and partnering of teams yielded a diverse suite of modeling approaches, insights to the nature of the Fenton Hill reservoirs, and conclusions. But this diversity has been ideal for defining near-term experimental and numerical research objectives. Moreover, the collaborative nature of the study's approach induced participants to challenge themselves and established approaches, through a concentrated and open exchange of numerical simulation results against experimental observations.

Acknowledgements This material was based upon work supported by the U.S. Department of Energy, Office of Energy Efficiency and Renewable Energy (EERE), Office of Technology Development, Geothermal Technologies Program, under Award Numbers DE-AC52-07NA27344 with LLNL, and under Award Number DE-AC05-76RL01830 with PNNL. The authors wish to acknowledge the pioneering scientists and engineers at Los Alamos Scientific Laboratory, whose tenacity and technical expertise contributed to the success of the Fenton Hill experiments, conducted over a 23-year period. We are especially grateful to Donald W. Brown, David V. Duchane, Grant Heiken, and Vivi Thomas Hriscu, for capturing these activities at Fenton Hill in great detail in their book "Mining the Earth's Heat: Hot Dry Rock Geothermal Energy." We would also personally like to thank Donald W. Brown for participating in this study's teleconferences and for engaging with the participants on technical issues.

Compliance with ethical standards

Conflict of interest Derek Elsworth is an editor-in-chief for the Geomechanics and Geophysics for Geo-Energy and Geo-Resources journal, otherwise on behalf of all authors, the corresponding author states that there is no conflict of interest.

References

- Bradford J et al (2013) Recent developments at the raft river geothermal field. In: Thirty-eighth workshop on geothermal reservoir engineering, Stanford University, Stanford, CA, February 11–13, 2013
- Bradford J et al (2015) Recent thermal and hydraulic stimulation results at raft river, ID EGS site. In: Fortieth workshop on geothermal reservoir engineering, Stanford, CA, USA, January 26–28, 2015. Stanford University
- Bahrami D, Danko G, Fu P, Guo B, Podgorney RK, White MD, Xia Y (2015) Poroelastic and self-propped single fracture THM models for EGS studies. In: Fortieth workshop on geothermal reservoir engineering, Stanford University, Stanford, CA, January 26–28, 2015
- Bandis SC, Lumsden AC, Barton NR (1983) Fundamentals of rock joint deformation. *Int J Rock Mech Min* 20:249–268. [https://doi.org/10.1016/0148-9062\(83\)90595-8](https://doi.org/10.1016/0148-9062(83)90595-8)
- Barton N, Bandis S, Bakhtar K (1985) Strength, deformation and conductivity coupling of rock joints. *Int J Rock Mech Min* 22:121–140. [https://doi.org/10.1016/0148-9062\(85\)93227-9](https://doi.org/10.1016/0148-9062(85)93227-9)
- Brown DW (1989) The potential for large errors in the inferred minimum earth stress when using incomplete hydraulic fracturing results. *Int J Rock Mech Min Sci Geomech Abstr* 26:573–577. [https://doi.org/10.1016/0148-9062\(89\)91437-X](https://doi.org/10.1016/0148-9062(89)91437-X)
- Brown DW, Duchane DV, Heiken G, Hriscu VT (2012) Mining the earth's heat: hot dry rock geothermal energy. Springer, New York. <https://doi.org/10.1007/978-3-540-68910-2>
- Chabora E et al (2012) Hydraulic stimulation of well 27-15, desert peak geothermal field, Nevada USA. In: 37th workshop on geothermal reservoir engineering, Stanford, CA, USA, January 1–February 30, 2012. Stanford University
- Danko G, Bahrami D (2013a) Dynamic model of discrete fracture opening under fluid injection. In: Thirty-eighth workshop on geothermal reservoir engineering, Stanford University, Stanford
- Danko G, Bahrami D (2013b) EGS model adaptation and forecasting studies with MULTIFLUX. *Geotherm Resour Counc Trans* 37:141–147
- Danko G, Bahrami D, Vazquez I (2016) Fracture and flow system modeling method for an EGS reservoir. In: Stanford geothermal workshop. Stanford University
- Deichmann N, Giardini D (2009) Earthquakes induced by the stimulation of an enhanced geothermal system below Basel (Switzerland). *Seismol Res Lett* 80:784–798. <https://doi.org/10.1785/gssrl.80.5.784>
- Dempsey D, Kelkar S, Lewis K, Hickman S, Davatzes N, Moos D, Zemach E (2013) Modeling shear stimulation of the desert peak EGS well 27-15 using a coupled thermal-hydrological-mechanical simulator. In: 47th U.S. rock mechanics/geomechanics symposium, San Francisco, CA, 2013/1/1/. American Rock Mechanics Association, ARMA
- Duchane DV (1996) Heat mining to extract hot dry rock geothermal energy: technical and scientific progress. In: Federal geothermal research program update, fiscal year 1995. U.S. Department of Energy, Washington, DC, USA
- Francesco RD (2013) Exact solution of Terzaghi's consolidation equation and extension to two/three-dimensional cases. *Appl Math* 4:713–717. <https://doi.org/10.4236/am.2013.440099>
- Fu P, McClure MW, Shiozawa S, White MD (2016) Revisiting Fenton Hill Phase 1 reservoir creation and stimulation mechanisms through the GTO code comparison study. Paper presented at the 50th U.S. rock mechanics/geomechanics symposium, Houston, TX, USA
- Gan Q, Elsworth D (2016) A continuum model for coupled stress and fluid flow in discrete fracture networks. *Geomech Geophys Geo Energy Geo Resour* 2:43–61. <https://doi.org/10.1007/s40948-015-0020-0>
- Gao Q, Ghassemi A (2016) 3D thermo-poromechanical analysis of reservoir stimulation using damage mechanics with application to the Fenton Hill HDR Experiment. In: 50th U.S. rock mechanics/geomechanics symposium, Houston, TX, USA
- Ghassemi A, Kelkar S, McClure MW (2015) Influence of fracture shearing on fluid flow and thermal behavior of an EGS reservoir-geothermal code comparison study. In: Fortieth workshop on geothermal reservoir engineering, Stanford University, Stanford, CA, January 26–28, 2015
- Holling CS (1978) Adaptive environmental assessment and management. Wiley, Chichester
- Huang H, Plummer M, Podgorney RK (2013) Simulated evolution of fractures and fracture networks subject to thermal cooling and fluid pressure changes: a coupled network flow and discrete element model. In: Thirty-eighth workshop on geothermal reservoir engineering, Stanford University, Stanford, CA, February 11–13, 2013
- Izutani Y, Kanamori H (2001) Scale-dependence of seismic energy-to-moment ratio for strike-slip earthquakes in Japan. *Geophys Res Lett* 28:4007–4010. <https://doi.org/10.1029/2001gl013402>
- Jeanloz R, Stone H (2013) Enhanced geothermal systems. The MITRE Corporation, Jason Program Office, McLean
- Kazemi H, Merrill LS, Porterfield KL, Zeman PR (1976) Numerical-simulation of water-oil flow in naturally fractured reservoirs. *Soc Petrol Eng J* 16:317–326
- Kelkar S, Murphy H, Dash Z (1986) Earth stress measurements in deep granitic rock. In: 27th U.S. symposium on rock mechanics, Tuscaloosa, AL, 1986
- Lee SH, Ghassemi A (2009) Thermo-poroelastic finite element analysis of rock deformation and damage. In: 43rd U.S. rock mechanics symposium and 4th U.S.-Canada rock mechanics symposium, Asheville, NC, USA, 2009
- Lemonnier P, Bourbiaux B (2010) Simulation of naturally fractured reservoirs. State of the art part I physical mechanisms and simulator formulation oil gas. *Sci Technol* 65:239–262. <https://doi.org/10.2516/ogst/2009066>
- Lichtner PC et al (2015) PFLOTRAN user manual: a massively parallel reactive flow and transport model for describing surface and subsurface processes. Los Alamos National Laboratory, Los Alamos
- Majer EL, Baria R, Stark M, Oates S, Bommer J, Smith B, Asanuma H (2007) Induced seismicity associated with enhanced geothermal systems. *Geothermics* 36:185–222. <https://doi.org/10.1016/j.geothermics.2007.03.003>

- McClure MW (2012) Modeling and characterization of hydraulic stimulation and induced seismicity in geothermal and shale gas reservoirs. Stanford University, Stanford
- McClure MW, Horne RN (2011) Investigation of injection-induced seismicity using a coupled fluid flow and rate/state friction model. *Geophysics* 76:Wc181–Wc198. <https://doi.org/10.1190/geo2011-0064.1->>
- McClure M, Horne RN (2013) Discrete fracture network modeling of hydraulic stimulation: coupling flow and geomechanics. Springer Briefs in Earth Sciences, 1st edn. Springer, New York. <https://doi.org/10.1007/978-3-319-00383-2>
- McClure MW, Horne RN (2014) An investigation of stimulation mechanisms in enhanced geothermal systems. *Int J Rock Mech Min* 72:242–260. <https://doi.org/10.1016/j.ijrmms.2014.07.011>
- McClure M, Babazadeh M, Shiozawa S, Huang J (2015) Fully coupled hydromechanical simulation of hydraulic fracturing in three-dimensional discrete fracture networks. In: Society of petroleum engineers, SPE, 2015/2/3. doi:<https://doi.org/10.2118/173354-MS>
- Molloy MW et al (1980) Geothermal reservoir engineering code comparison project. In: Special panel on geothermal model intercomparison study, 6th workshop on geothermal reservoir engineering, Stanford University, Stanford, CA, USA
- Mudunuru M, Kelkar S, Karra S, Harp D, Guthrie G, Viswanathan H (2016) Reduced-order models to predict thermal power output for enhanced geothermal systems. In: Stanford geothermal workshop, Stanford University, 2016
- Murphy HD, Tester JW, Grigsby CO, Potter RM (1981) Energy extraction from fractured geothermal reservoirs in low-permeability crystalline rock. *J Geophys Res Solid Earth* 86:7145–7158. <https://doi.org/10.1029/JB086iB08p07145>
- Mutlu O, Pollard DD (2008) On the patterns of wing cracks along an outcrop scale flaw: a numerical modeling approach using complementarity. *J Geophys Res Solid Earth*. <https://doi.org/10.1029/2007JB005284>
- Nathenson M (1999) The dependence of permeability on effective stress from flow tests at hot dry rock reservoirs at Rosemanowes (Cornwall) and Fenton Hill (New Mexico). *Geothermics* 28:315–340. [https://doi.org/10.1016/S0375-6505\(99\)00011-5](https://doi.org/10.1016/S0375-6505(99)00011-5)
- Noorishad J, Tsang CF, Witherspoon PA (1984) Coupled thermal-hydraulic-mechanical phenomena in saturated fractured porous rocks—numerical approach. *J Geophys Res* 89:365–373. <https://doi.org/10.1029/JB089iB12p10365>
- Norbeck J (2016) Hydromechanical and frictional faulting behavior of fluid-injection-induced earthquakes. Stanford University, Stanford
- Norbeck JH, Horne RN (2016) A numerical method for fractured reservoir poromechanics using a mixed-continuum embedded fracture model. Paper presented at the Geothermal Resources Council Transactions, Sacramento, California, USA
- Norbeck J, McClure M, Horne R (2016a) Revisiting stimulation mechanism at Fenton Hill and an investigation of the influence of fault heterogeneity on the Gutenberg-Richter b-value for rate-and-state earthquake simulations. In: Stanford geothermal workshop, Stanford University
- Norbeck JH, McClure MW, Horne RN (2016b) Revisiting stimulation mechanism at Fenton Hill and an investigation of the influence of fault heterogeneity on the Gutenberg-Richter b-value for rate-and-state earthquake simulations. In: 41st Workshop on geothermal reservoir engineering, Stanford University, Stanford, CA, USA
- Norbeck JH, McClure MW, Lo JW, Horne RN (2016c) An embedded fracture modeling framework for simulation of hydraulic fracturing and shear stimulation. *Comput Geosci* 20:1–18. <https://doi.org/10.1007/s10596-015-9543-2>
- Phillips WS, House LS, Fehler MC (1997) Detailed joint structure in a geothermal reservoir from studies of induced microearthquake clusters. *J Geophys Res Solid Earth* 102:11745–11763. <https://doi.org/10.1029/97jb00762>
- Pollard DD, Holzhausen G (1979) On the mechanical interaction between a fluid-filled fracture and the earth's surface. *Tectonophysics* 53:27–57. [https://doi.org/10.1016/0040-1951\(79\)90353-6](https://doi.org/10.1016/0040-1951(79)90353-6)
- Roff A, Phillips WS, Brown DW (1996) Joint structures determined by clustering microearthquakes using waveform amplitude ratios. *Int J Rock Mech Min Sci Geomech Abstr* 33:627–639. [https://doi.org/10.1016/0148-9062\(95\)00077-1](https://doi.org/10.1016/0148-9062(95)00077-1)
- Rutqvist J (2017) An overview of TOUGH-based geomechanics models. *Comput Geosci* (in Press). doi:<https://doi.org/10.1016/j.cageo.2016.09.007>
- Rutqvist J, Wu YS, Tsang CF, Bodvarsson G (2002) A modeling approach for analysis of coupled multiphase fluid flow, heat transfer, and deformation in fractured porous rock. *Int J Rock Mech Min* 39:429–442. [https://doi.org/10.1016/S1365-1609\(02\)00022-9](https://doi.org/10.1016/S1365-1609(02)00022-9)
- Rutqvist J et al (2015) The Northwest Geysers EGS demonstration project, California: pre-stimulation modeling and interpretation of the stimulation. *Math Geosci* 47:3–29. <https://doi.org/10.1007/s11004-013-9493-y>
- Scheibe TD, White MD, White SK (2013) Outcomes of the 2013 TO workshop on geothermal code comparison. Pacific Northwest National Laboratory, Richland
- Shiozawa S, McClure M (2016) Simulation of proppant transport with gravitational settling and fracture closure in a three-dimensional hydraulic fracturing simulator. *J Petrol Sci Eng* 138:298–314. <https://doi.org/10.1016/j.petrol.2016.01.002>
- Smith MC, Hendron RH, Murphy HD, Wilson MG (1989) Hot dry rock geothermal energy development program. Annual report, fiscal year 1987. Los Alamos National Laboratory, Los Alamos, NM, USA
- Starfield AM, Cundall PA (1988) Towards a methodology for rock mechanics modeling. *Int J Rock Mech Min Sci Geomech Abstr* 25:99–106. [https://doi.org/10.1016/0148-9062\(88\)92292-9](https://doi.org/10.1016/0148-9062(88)92292-9)
- Steeffel CI, Lasaga AC (1994) A coupled model for transport of multiple chemical-species and kinetic precipitation dissolution reactions with application to reactive flow in single-phase hydrothermal systems. *Am J Sci* 294:529–592
- Taron J, Elsworth D, Min K-B (2009) Numerical simulation of thermal-hydrologic-mechanical-chemical processes in deformable, fractured porous media. *Int J Rock Mech Min* 46:842–854. <https://doi.org/10.1016/j.ijrmms.2009.01.008>

- Tehrani MA (1996) An experimental study of particle migration in pipe flow of viscoelastic fluids. *J Rheol* 40:1057–1077. <https://doi.org/10.1122/1.550773>
- Verma A, Pruess K (1988) Thermohydrological conditions and silica redistribution near high-level nuclear wastes emplaced in saturated geological formations. *J Geophys Res Solid* 93:1159–1173. <https://doi.org/10.1029/JB093iB02p01159>
- Warren JE, Root PJ (1963) The behavior of naturally fractured reservoirs. *Soc Petrol Eng J* 3:245–255
- White MD, Phillips BR (2015) Code comparison study fosters confidence in the numerical simulation of enhanced geothermal systems. In: Fortieth workshop on geothermal reservoir engineering, Stanford University, Stanford, CA, January 26–28, 2015
- White SK, Purohit S, Boyd L (2015) Using GTO-Velo to facilitate communication and sharing of simulation results in support of the geothermal technologies office code comparison study. In: Fourtieth workshop on geothermal reservoir engineering, Stanford University, Stanford, CA, January 26–28, 2015
- White MD, Elsworth D, Sonnenthal E, Fu P, Danko G (2016a) Challenge problem statements for a code comparison on the Fenton Hill Reservoir—an invitation to the geothermal modeling community. In: Stanford geothermal workshop, Stanford University
- White MD et al (2016b) Benchmark problems of the geothermal technologies office code comparison study. Pacific Northwest National Laboratory, Richland. <https://doi.org/10.2172/1337724>
- White MD et al (2017) Challenge problems of the geothermal technologies office code comparison study. Pacific Northwest National Laboratory, Richland
- Wood WW (2009) Enhanced geothermal systems: an opportunity for hydrogeology. *Ground Water* 47:751. <https://doi.org/10.1111/j.1745-6584.2009.00573.x>
- Xu T, Pruess K (2004) Numerical simulation of injectivity effects of mineral scaling and clay swelling in a fractured geothermal reservoir. Lawrence Berkeley National Laboratory. <https://escholarship.org/uc/item/8rz736j9>
- Xu TF, Apps JA, Pruess K (2004) Numerical simulation of CO₂ disposal by mineral trapping in deep aquifers. *Appl Geochem* 19:917–936. <https://doi.org/10.1016/j.apgeochem.2003.11.003>
- Zoback MD (2007) Reservoir geomechanics. Cambridge University Press, Cambridge